

Selective activation of C-H bonds in a Cascade Process Combining photochemistry with biocatalysis

Wuyuan Zhang^{1†}, Bastian O. Burek^{2†}, Elena Fernández-Fueyo³, Miguel Alcalde⁴, Jonathan Z. Bloh^{2*}, Frank Hollmann^{1*}

Affiliations:

¹Department of Biotechnology, Delft University of Technology, Van der Maasweg 9, 2629HZ Delft, The Netherlands.

² DECHEMA-Forschungsinstitut, Theodor-Heuss-Allee 25, 60486 Frankfurt am Main, Germany.

³ Centro de Investigaciones Biológicas, Consejo Superior de Investigaciones Científicas (CSIC), Madrid, Spain.

⁴ Department of Biocatalysis, Institute of Catalysis, Consejo Superior de Investigaciones Científicas (CSIC), 28049 Madrid, Spain.

*Correspondence to: f.hollmann@tudelft.nl; bloh@dechema.de

†Both authors contributed equally.

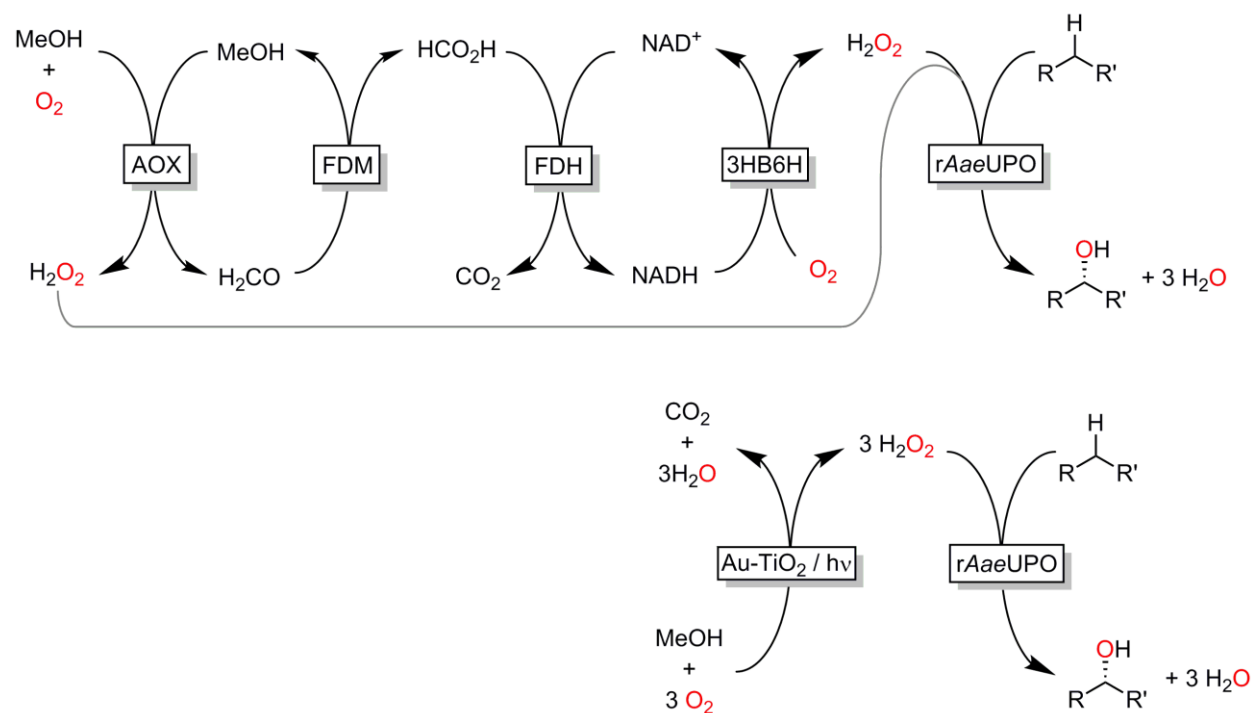
Abstract: Selective oxyfunctionalisation of inert C-H bonds under mild conditions can be achieved using peroxygenases as catalysts. This approach, however, is impaired by the poor robustness of these enzymes in the presence of hydrogen peroxide as the stoichiometric oxidant. Here, we demonstrate that inorganic photocatalysts such as gold-titanium dioxide efficiently provide H₂O₂ from methanol-driven reductive activation of ambient oxygen in suitable amounts to ensure high reactivity and robustness of the enzyme. This unique combination of inorganic photocatalysis and biocatalytic oxyfunctionalisation chemistry combines the best of both worlds to efficiently produce a range of (chiral) alcohols from the corresponding hydrocarbons.

One Sentence Summary: Selective oxyfunctionalisation reactions are achieved by combining inorganic photocatalysis with selective enzymatic oxyfunctionalisation catalysis.

Selective oxyfunctionalisation of (non-)activated C-H bonds still represents one of the major challenges in organic synthesis. Heme-dependent oxygenases are valuable catalysts for this task as they confine highly reactive Fe(IV)O species in the sterically well-defined active site of an enzyme.(1, 2) Today, mostly P450 monooxygenases are considered as biocatalysts but peroxygenases (E.C.1.11.2.1) represent a practical alternative especially due to their ease of application. Instead of relying on complex electron supply chains providing the enzymes with reducing equivalents as in case of P450 monooxygenases, peroxygenases use hydrogen peroxide (H₂O₂) directly to form the catalytically active oxyferryl species (Compound I).(3)

H₂O₂, however, also is a potent inactivator of heme-dependent enzymes via oxidative decomposition of the heme-prosthetic group. Therefore, *in situ* generation of H₂O₂ in low concentrations is the preferred approach to alleviate this challenge.(2) Generally, this is achieved through *in situ* reduction of O₂ to H₂O₂, posing the question about the nature of the sacrificial electron donor used for this reaction. Next to electrochemical methods(4, 5) oxidation of stoichiometric cosubstrates such as EDTA, amino acids, alcohols and other reductants(2) have been investigated. Today, the most common system for *in situ* generation of H₂O₂ certainly is glucose/glucose oxidase. The poor atom efficiency of this system (glucose is oxidised only once to the corresponding lactone generating one equivalent of H₂O₂) together with the edibility of glucose pose significant technological and ethical challenges to this approach (especially if used at preparative scale). In style of the industrial anthraquinone process(6) hydrogenation of molecular oxygen to H₂O₂ would represent a very interesting, since atom-efficient, process, which practically however is challenged by safety issues. Therefore, we recently reported an enzymatic cascade to fully oxidize methanol to CO₂ and utilize the reduction equivalents liberated for H₂O₂ generation to promote peroxygenase reactions (Scheme 1). (7) For this, a rather complicated cascade comprising four enzymes and one cofactor was established. Despite the success of this reaction system, we asked ourselves whether a simpler and more elegant *in situ* H₂O₂ generation method is possible.

Inspired by so recent works by Choi and Tada,(8, 9) we set out to evaluate the application of gold-loaded TiO₂ as plasmonic photocatalyst for the photochemical oxidation of methanol coupled to reductive activation of molecular oxygen to promote peroxygenase-catalysed oxyfunctionalisation reactions (Scheme 1).



Scheme 1. Comparison of the previously reported *in situ* H_2O_2 generation to promote peroxygenase-catalysed hydroxylation of alkanes using the recombinant peroxygenase from *Agrocybe aegerita* (*rAaeUPO*). Upper: the previously reported multi-enzyme cascade comprising alcohol oxidase (AOx), formaldehyde dismutase (FDM), formate dehydrogenase (FDH), 3-hydroxy benzoate-6-hydroxylase (3HB6H) as well as the nicotinamide cofactor (NADH/NAD^+); lower: photochemical oxidation of methanol using Au-doped TiO_2 (Au-TiO_2).

Results

To test our hypothesis, we first synthesized Au-loaded TiO_2 (rutile phase)(10) as methanol oxidation catalyst (SI for details) and used it for the selective hydroxylation of ethyl benzene to (*R*)-1-phenyl ethanol catalysed by the recombinant evolved peroxygenase from *Agrocybe aegerita* (*rAaeUPO*) as model reaction.(11)

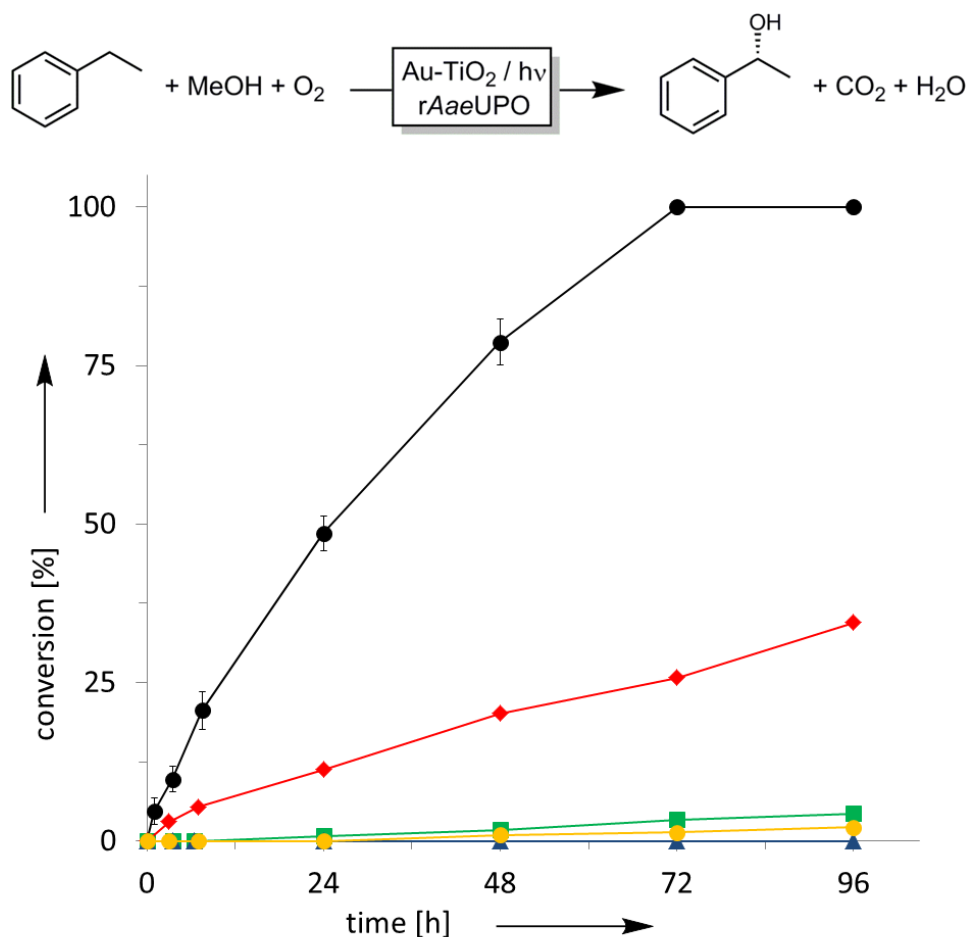


Figure 1. Photochemoenzymatic hydroxylation of ethyl benzene to (*R*)-1-phenyl ethanol combining Au-TiO₂ as photocatalyst for *in situ* H₂O₂ generation and rAaeUPO for the stereospecific hydroxylation reaction (●). Negative controls excluding enzyme (■), light (▲), methanol (◆) or rutile Au-TiO₂ (●). Reaction conditions: [methanol] = 250 mM, [rutile Au-TiO₂] = 5 mg mL⁻¹, [rAaeUPO] = 150 nM and [ethylbenzene] = 15 mM in 60 mM phosphate buffer (pH 7.0) under visible light illumination ($\lambda > 400$ nm).

Quite pleasingly, the proof-of-concept reaction proceeded smoothly to full conversion. Overall 10.7 mM of (*R*)-1-phenylethanol (98.2 % ee) was obtained within 72h corresponding to a turnover number ($TN = \text{mol}_{\text{product}} \times \text{mol}_{\text{catalyst}}^{-1}$) of more than 71.000 for the biocatalyst. The sole by-product detectable was trace amounts of acetophenone originating from the over-oxidation of the product by rAaeUPO (commencing upon depletion of the starting material). Omitting the biocatalyst resulted in small amounts (<0.15 mM) of racemic 1-phenyl ethanol. In the absence of the photocatalyst or performing the reactions in the darkness resulted in no detectable product

formation. In the absence of methanol, some product formation was observed, which we attribute to Au-TiO₂-catalyzed water oxidation (Zhang et al unpublished).

It should be emphasized that the present reaction setup (open reactor with direct contact to the ambient atmosphere) suffered from some evaporation issues accounting for approx. 10-20% loss of reagents. Optimised setups, particularly closed vessels, will circumvent this apparent limitation.

Next, we systematically investigated the influence of the single reagents on the rate of the photoenzymatic hydroxylation reaction (Table 1, and Figures S9-21).

Table 1. Photochemical *in situ* H₂O₂ generation to promote peroxygenase catalysed oxyfunctionalisation reaction.^[a]

	electron donor	[rAaeUPO] [nM]	[electron donor] [mM]	[Au-TiO ₂] [g L ⁻¹]	Initial rate [mM h ⁻¹]	Steady-state [H ₂ O ₂] [μM] ^[b]	[(R)-1-phenyl ethanol] [mM] ^[c]	Yield [%] ^[d]	Conversion [%] ^[e]	TON (rAaeUPO) × 10 ³ ^[f]	
				Product	H ₂ O ₂						
1	MeOH	150	0	5	0.17	0.37	42	2.9	19	26	19
2	MeOH	150	5	5	0.20	0.56	55	3.3	22	24	22
3	MeOH	150	50	5	0.26	0.28	128	5.9	39	71	39
4	MeOH	150	100	5	0.24	0.56	231	6.4	42	76	42
5	MeOH	150	250	5	0.45	0.52	156	10.7	71	>99	71
6	MeOH	150	500	5	0.46	n.d.	n.d.	10.4	69	97	69
7	MeOH	50	250	5	0.27	0.52	156	2.8	18	36	55
8	MeOH	350	250	5	0.47	0.52	156	10.7	72	97	31
9	MeOH	150	250	10	0.46	1.05	160	11.9	79	>99	79
10	MeOH	150	250	20	0.29	0.44	97	10.1	67	>99	67
11	HCHO	250	150	5	0.73	1.01 ^[g]	1050 ^[g]	13.7	91	>99	91
12	NaHCO ₂	250	150	5	0.58	0.98 ^[g]	193 ^[g]	12.6	84	99	84
13	EtOH	250	150	5	0.20	0.32 ^[h]	154 ^[h]	3.8	25	33	25
14	ⁱ PrOH	250	150	5	0.26	0.36 ^[h]	122 ^[h]	5.3	35	46	35

[a] reaction conditions: [ethylbenzene] = 15 mM in 60 mM phosphate buffer (pH 7.0) at 30 °C for 72 hours under visible light illumination ($\lambda > 400$ nm); [b] as determined in comparative experiments illuminating Au-TiO₂ in the reaction buffer (Figures S11, S14, S18 and S21); n.d. = not determined. [c] Product with 98% ee was obtained unless indicated otherwise. [d] yield = [(R)-1-phenyl ethanol]_{final} × 15 mM⁻¹; [e] conversion = [(R)-1-phenyl ethanol]_{final} × ((R)-1-phenyl ethanol]_{final} + [ethyl benzene]_{final})⁻¹; [f] TON = [(R)-1-phenyl ethanol]_{final} × [rAaeUPO]⁻¹; [g] determined at 100 mM of the sacrificial reductant; [h] determined at 250 mM of the sacrificial reductant.

The concentration of MeOH had a significant effect on the initial rate steadily increasing with [MeOH] (Table 1, entries 1-6) and correlating well with the increasing formation rate and steady-state concentrations of H₂O₂. Au-TiO₂ is known to also oxidise H₂O₂ thereby preventing its continuous accumulation in the reaction mixture.(8, 12) Hence, both H₂O₂ and MeOH compete for oxidation at the catalyst surface which explains the higher steady state concentration of H₂O₂ in the presence of methanol. Above approx. 250 mM MeOH the photocatalyst surface appeared to be fully saturated as no further increase in product formation rate was observed. It is also worth mentioning here that MeOH not only increased the overall reaction rate but also positively influenced the robustness of the process (*vide infra*).

In terms of photocatalyst concentration there seemed to be an optimal value around approx. 10 g L⁻¹ with respect to the rate of the photoenzymatic hydroxylation reaction (Table 1, entries 5, 9 and 10). This observation may be a bit counter-intuitive at first sight but becomes apparent considering the optical transparency of the corresponding reaction mixtures (Figures S22-23). Hence, the increasing H₂O₂ generation activity with increasing photocatalyst concentration was counteracted by the decreasing transparency of the reaction mixtures leading to poorer light penetration into the reaction mixture and consequently to a lower fraction of illuminated and therefore active photocatalyst. Again, there was a good correlation between the overall rate with the steady state H₂O₂ concentration.

Increasing the enzyme concentration above 150 nM resulted in no further increase of the overall reaction rate (Table 1, entries 5, 7 and 8). A plausible explanation is that above this value the system was entirely H₂O₂-limited, *i.e.* almost every H₂O₂ molecule generated was consumed productively by the enzyme. Since the H₂O₂ formation rate under these conditions was 0.52 mM h⁻¹ and the initial enzymatic product formation rate was 0.45 mM h⁻¹, the efficiency for the enzymatic H₂O₂ utilization was approximately 87%. As a consequence only about 13% of the H₂O₂ provided by the photocatalyst was wasted due to photocatalytic or enzymatic (catalase activity) degradation. On the contrary, when the enzyme concentration was decreased to a third, the reaction rate was approximately halved, indicating that H₂O₂ was no longer the (sole) limiting factor. Under these conditions, the H₂O₂ utilization efficiency dropped to 52%, as not all of the peroxide was consumed by the enzyme anymore and the excess was degraded by the photocatalyst and other unproductive processes.

The photon flux inside the reaction vessel, determined using ferrioxalate actinometry(13) was 2851 mE L⁻¹ h⁻¹. Consequently, under standard conditions (150nM UPO, 250mM methanol) the photonic efficiencies of hydrogen peroxide and (*R*)-1-phenyl ethanol formation were 0.036% and 0.032%, respectively. Assuming that only fraction of light corresponding to the band gap of the rutile photocatalyst ($\geq 3\text{eV} / \leq 413\text{nm}$, 0.7% of the lamp intensity, see SI) was responsible for the activity, a photonic efficiency of 5.2% for hydrogen peroxide and 4.5% for the enzymatic conversion product can be estimated, respectively. In view of previously reported photonic efficiencies of only 1% for TiO₂(14) this may suggest that the photocatalyst used here could also harvest some of the visible fraction as well, presumably via the gold plasmonic resonance at approximately 550-600 nm (Figure S5).

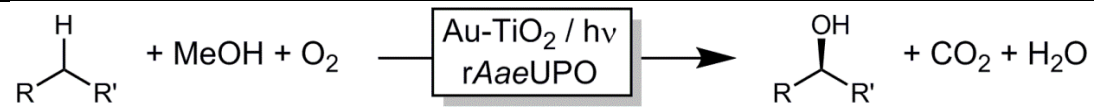
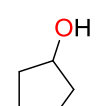
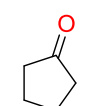
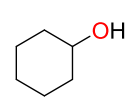
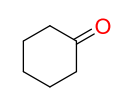
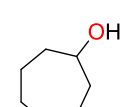
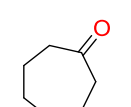
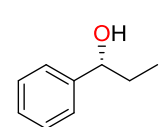
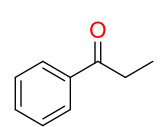
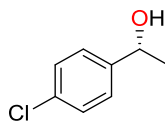
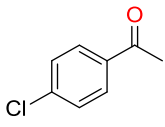
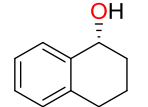
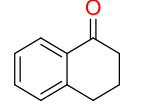
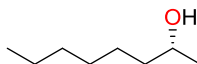
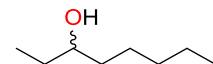
¹H NMR analysis revealed that the Au-TiO₂-catalysed oxidation of methanol did not stop at the formaldehyde level but also produced formic acid and, presumably, CO₂ (Figures S25-26). To further investigate this (desired) overoxidation of methanol, a set of experiments was conducted substituting methanol with formaldehyde and formate, respectively, under otherwise identical conditions (Table 1, entries 11, 12). Formaldehyde and formate gave approximately 32% and 18% faster reaction rates than methanol, respectively. This can be readily explained by the higher hydrogen peroxide formation rates observed for these compounds, both showed about 75% higher H₂O₂ formation rates. Formaldehyde also suppressed H₂O₂ degradation, resulting in a higher steady state concentration of H₂O₂. The fact that the increase in peroxide formation was somewhat diminished in the enzymatic reaction rate might be explained by two effects. On the one hand, the response of the enzyme to a higher H₂O₂ formation rate is non-linear, as at some point the enzyme approaches its maximum turnover rate. On the other hand, the experiments with methanol are automatically superimposed by the reaction rate of formaldehyde and formate as they are formed during the reaction. This would be more pronounced in the photoenzymatic experiments than in the photocatalytic H₂O₂ formation due to the longer timescale of the experiments which allow for a higher fraction of the methanol to be converted.

So far, only methanol has been used as sacrificial electron donor for the photochemoenzymatic reaction. Also other alcohols such as ethanol or isopropanol could be used as sacrificial electron donors to promote the overall reaction, albeit at lower rates as compared to methanol (Table 1, entries 13, 14). The relative rates found with ethanol and isopropanol are in good correlation with

the steady-state concentration and formation rate of H₂O₂ and roughly correlate with the oxidation potentials of the alcohols.⁽¹⁵⁾

Finally, we also evaluated the substrate scope of the proposed photochemobiocatalytic reaction sequence (Table 2). In line with the reported substrate scope of rAaeUPO⁽¹⁶⁾ a range of (cyclo)alkanes and alkylaromatic compounds were converted into the corresponding alcohols. The regio- and enantioselectivity was essentially the same as in previous studies. The only side reaction observed was a minor overoxidation to the corresponding ketone. On the one hand, this may be attributed to photocatalytic oxidation by Au-TiO₂. On the other hand, also rAaeUPO is capable of this reaction.

Table 2. Preliminary substrate scope of the photochemobiocatalytic hydroxylation reaction.^[a]

							
Entry	product	mM	ee [%]	Other products	mM	Yield, ^[b] %	TON, 10 ³
1		6.6	/		0.5	66	43.9
2		9.2	/		0.3	92.3	61.5
3		4.3	/		0.4	43	28.6
4		6.9	>99		1.6	68.7	45.8
5		8.9	95.0		1.6	89.4	59.6
6		8.0	93.3		1.3	80.2	53.5
7		1.0	89		1.6	26	17.5

^[a] Conditions: [substrate] = 10.0 mM, [rutile Au-TiO₂] = 10 gL⁻¹, [rAaeUPO] = 150 nM, [MeOH] = 250 mM in phosphate buffer (pH 7.0, 60 mM), T = 30 °C, 70 h, visible light illumination ($\lambda > 400$ nm). ^[b] based on the concentration of both products.

Very pleasingly, high turnover numbers could be achieved throughout these experiments that compare well with the numbers reported so far with more complicated *in situ* H₂O₂ generation systems.⁽²⁾ Hence, we are optimistic that further optimisation of the reaction setup may well lead to an economically attractive oxyfunctionalisation reaction. Indeed, a semi-preparative scale hydroxylation reaction of ethyl benzene yielded more than 100 mg of essentially enantiopure product in an isolated yield of 51%. Further optimisation is currently underway.

As mentioned above, methanol not only accelerated the overall reaction but also contributed to its robustness (Figure S24). We suspected the enzyme to be oxidatively inactivated by reactive oxygen species originating from water oxidation. Indeed, while illumination of rAaeUPO in the presence of Au-TiO₂ lead to almost immediate inactivation of the biocatalyst it retained almost 50% of its initial activity under the same conditions albeit in the presence of 250 mM (Figure S25). Analysing the reaction mixtures with the electron paramagnetic resonance (EPR) spin trap technique⁽¹⁷⁾ (Figure 2) qualitatively revealed the occurrence of both hydroxyl- and methoxyl-radicals. More quantitatively, the coumarin method⁽¹⁸⁾ showed that hydroxyl radicals were formed in significant amounts only in the absence of methanol (Figure 2). Upon addition of methanol (250 mM) the hydroxyl radical formation rate drops to only 0.6% of the original value.

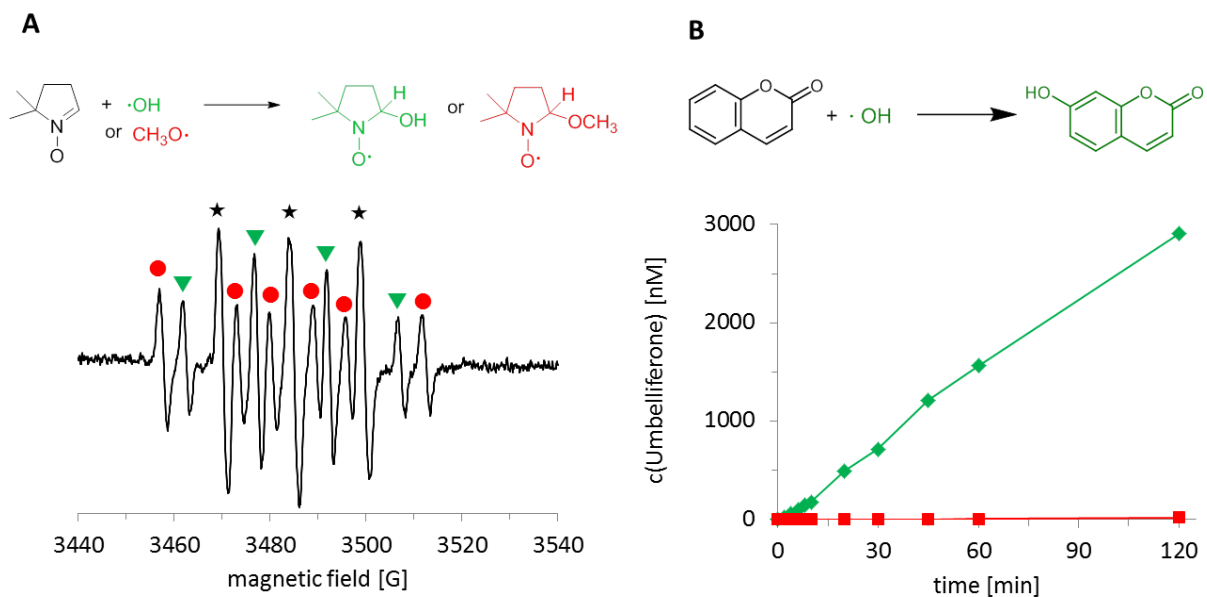


Figure 2. Qualitative and quantitative determination of radicals occurring during the photocatalytic process. (A) EPR spectra recorded during the illumination of and rutile Au-TiO₂ in water with methanol for 20 min. Signals marked with asterisk (★) belong to the existing oxidation product of DMPO, 5,5-dimethyl-2-oxopyrroline-1-oxyl (DMPOX).⁽¹⁹⁾ Signals marked with triangles (▼) belong to the spin-adduct •DMPO-OH. Signals marked with circles (●) belong to the spin-adduct •DMPO-CH₂OH from methanol.⁽¹⁷⁾ Reaction condition: [Au-TiO₂] = 5 g L⁻¹, [DMPO] = 30 mM, [methanol]= 100 mM, RT, hv > 400 nm; (B) Time course of the photocatalytic umbelliferone generation from coumarin as a specific detection method for •OH radicals. Reaction conditions: 60 mM phosphate buffer (pH 7), [Au-TiO₂] = 5 g L⁻¹, [coumarin] = 0.1 mM, [methanol]= 0 (■) or 250 mM (◆), RT, hv > 400 nm.

Apparently, methanol oxidation occurs significantly faster than water oxidation, which is comprehensible considering the redox potentials of water to hydroxyl radicals, +2.8 V,⁽²⁰⁾ and methanol to methanol radicals, +1.2 V,⁽²¹⁾ respectively. Moreover, due to the strong reducing nature of the methanol radical (-1.3 V), it can readily inject an electron into TiO₂, forming formaldehyde and resulting in up to two conduction band electrons per reactive photon, an effect also known as current doubling.⁽²²⁾ Hence, methanol oxidation not only accelerated the H₂O₂ generation rate but also prevented the formation of ROS thereby making the photobiocatalytic reaction more robust.

Overall, this study demonstrates the facile application of methanol as sacrificial reductant for *in situ* H₂O₂ generation from O₂ to promote selective, peroxygenase-catalysed oxyfunctionalisation reactions.

References and Notes:

1. There is only one reference list spanning the text, figure captions and supplementary materials. Do not include a second reference list in the supplementary materials section. Reference only cited in the supplementary materials section are not counted toward length guidelines.
2. Each reference should be on a separate line ending in a period. For a style guide, see www.sciencemag.org/about/authors/prep/res/refs.xhtml .
3. You can include titles in references and full page ranges. Titles are not counted toward length guidelines
4. Please include the above heading “References and Notes:”
5. You can use a numbered list in Word.
6. Each references should have a separate number.
7. Please do not mix in references with explanatory notes.

Acknowledgments: F.H and W.Z. gratefully acknowledge financial support by the European Research Council (ERC Consolidator Grant No. 648026). B.O.B and J.Z.B are grateful for financial support from the German Research Foundation (DFG, grant no. BL 1425/1-1).

Supplementary Materials:

This section includes the actual text of the Supplementary Materials, which can include any or all of the preceding items, and figure captions and tables that can easily be incorporated into one supplementary material file. Please edit the list above as appropriate and include it at the end of your main paper. If there are additional files that cannot be easily accommodated (e.g., movies or large tables), please include captions here.

Materials and Methods: Can include the Materials and Methods here. Additional references should be cited here and included in the main reference list.

Any Additional Author notes: For example, author contributions or a list of group authors.

1. Y. Wang, D. Lan, R. Durrani, F. Hollmann, Peroxygenases en route to becoming dream catalysts. What are the opportunities and challenges? *Curr. Opin. Chem. Biol.* **37**, 1-9 (2017).
2. S. Bormann, A. Gomez Baraibar, Y. Ni, D. Holtmann, F. Hollmann, Specific oxyfunctionalisations catalysed by peroxygenases: opportunities, challenges and solutions. *Catal. Sci. Technol.* **5**, 2038-2052 (2015).
3. M. Hofrichter, R. Ullrich, Oxidations catalyzed by fungal peroxygenases. *Curr. Opin. Chem. Biol.* **19**, 116-125 (2014).
4. D. S. Choi *et al.*, Photoelectroenzymatic Oxyfunctionalization on Flavin-Hybridized Carbon Nanotube Electrode Platform. *ACS Catal.* **7**, 1563-1567 (2017).
5. L. Getrey, T. Krieg, F. Hollmann, J. Schrader, D. Holtmann, Enzymatic halogenation of the phenolic monoterpenes thymol and carvacrol with chloroperoxidase. *Green Chem.* **16**, 1104-1108 (2014).
6. J. M. Campos-Martin, G. Blanco-Brieva, J. L. G. Fierro, Hydrogen Peroxide Synthesis: An Outlook beyond the Anthraquinone Process. *Angew. Chem. Int. Ed.* **45**, 6962-6984 (2006).
7. Y. Ni *et al.*, Peroxygenase-catalyzed oxyfunctionalization reactions promoted by the complete oxidation of methanol. *Angew. Chem. Int. Ed.* **55**, 798-801 (2016).
8. G. H. Moon, W. Kim, A. D. Bokare, N. E. Sung, W. Choi, Solar production of H₂O₂ on reduced graphene oxide-TiO₂ hybrid photocatalysts consisting of earth-abundant elements only. *Energ. Environ. Sci.* **7**, 4023-4028 (2014).
9. M. Teranishi, R. Hoshino, S.-I. Naya, H. Tada, Gold-nanoparticle-loaded carbonate-modified Titanium(IV) oxide surface: visible-light-driven formation of hydrogen peroxide from oxygen. *Angew. Chem. Int. Ed.* **55**, 12773-12777 (2016).
10. J. B. Priebe *et al.*, Solar hydrogen production by plasmonic Au-TiO₂ catalysts: impact of synthesis protocol and TiO₂ phase on charge transfer efficiency and H₂ evolution rates. *ACS Catal.* **5**, 2137-2148 (2015).
11. P. Molina-Espeja, S. Ma, D. M. Mate, R. Ludwig, M. Alcalde, Tandem-yeast expression system for engineering and producing unspecific peroxygenase. *Enz. Microb. Technol.* **73-74**, 29-33 (2015).
12. X. Z. Li, C. C. Chen, J. C. Zhao, Mechanism of photodecomposition of H₂O₂ on TiO₂ surfaces under visible light irradiation. *Langmuir* **17**, 4118-4122 (2001).
13. C. G. Hatchard, C. A. Parker, A NEW SENSITIVE CHEMICAL ACTINOMETER .2. POTASSIUM FERROXALATE AS A STANDARD CHEMICAL ACTINOMETER. *Proceedings of the Royal Society of London Series a-Mathematical and Physical Sciences* **235**, 518-536 (1956).
14. C. Kormann, D. W. Bahnemann, M. R. Hoffmann, PHOTOCATALYTIC PRODUCTION OF H₂O₂ AND ORGANIC PEROXIDES IN AQUEOUS SUSPENSIONS OF TiO₂, ZnO, AND DESERT SAND. *Environmental Science & Technology* **22**, 798-806 (1988).
15. J. Schneider *et al.*, Understanding TiO₂ photocatalysis: mechanisms and materials. *Chem. Rev.* **114**, 9919-9986 (2014).
16. S. Peter, M. Kinne, R. Ullrich, G. Kayser, M. Hofrichter, Epoxidation of linear, branched and cyclic alkenes catalyzed by unspecific peroxygenase. *Enz. Microb. Technol.* **52**, 370-376 (2013).

17. D. Dvoranová, Z. Barbieriková, V. Brezová, Radical intermediates in photoinduced reactions on TiO₂ (an EPR spin trapping study). *Molecules* **19**, 17279 (2014).
18. J. Zhang, Y. Nosaka, Quantitative Detection of OH Radicals for Investigating the Reaction Mechanism of Various Visible-Light TiO₂ Photocatalysts in Aqueous Suspension. *J. Phys. Chem. C* **117**, 1383-1391 (2013).
19. P. Bilski, K. Reszka, M. Bilska, C. F. Chignell, Oxidation of the spin trap 5,5-Dimethyl-1-pyrroline N-oxide by singlet oxygen in aqueous solution. *J. Am. Chem. Soc.* **118**, 1330-1338 (1996).
20. P. Wardman, REDUCTION POTENTIALS OF ONE-ELECTRON COUPLES INVOLVING FREE-RADICALS IN AQUEOUS-SOLUTION. *Journal of Physical and Chemical Reference Data* **18**, 1637-1755 (1989).
21. W. H. Koppenol, J. D. Rush, REDUCTION POTENTIAL OF THE CO₂/CO₂⁻ COUPLE - A COMPARISON WITH OTHER C1 RADICALS. *Journal of Physical Chemistry* **91**, 4429-4430 (1987).
22. J. Schneider, D. W. Bahnemann, Undesired Role of Sacrificial Reagents in Photocatalysis. *Journal of Physical Chemistry Letters* **4**, 3479-3483 (2013).

Supplementary Materials for

Selective activation of C-H bonds in a Cascade Process Combining photochemistry with Biocatalysis

Wuyuan Zhang, Bastien O. Burek, Elena Fernández-Fueyo, Miguel Alcalde, Jonathan Z. Bloh,
Frank Hollmann*

correspondence to: f.hollmann@tudelft.nl (F.H.) and bloh@dechema.de (JZB)

This PDF file includes:

Materials and Methods

Figs. S1 to S37

Tables S1 to S2

Materials and Methods

Chemicals

Unless otherwise mentioned, all chemicals were purchased from Sigma-Aldrich, Fluka, Acros or Alfa-Aesar with the highest purity available and used without further treatment. Titanium (IV) oxide (pure rutile phase) were brought from Sigma-Aldrich (the Netherlands) and used as received. Please note that the rutile TiO₂ was synthesized via gas phase method as it was confirmed by the supplier. The anatase TiO₂ herein contains mixed phase of rutile and anatase (9 : 91). Gold(III) chloride (64.4% minimum) was brought from Alfa-Aesar.

Preparation of the photocatalysts Au-TiO₂

The procedures were adapted from previous procedures.(1, 2) In order to deposit Au nanoparticles onto the surface of TiO₂, the so-called deposition-precipitation method was carried out as following: an aqueous solution of AuCl₃ (5 mM, slight yellow) was firstly heated to 70 °C. The pH of this solution was adjusted to 7.2 by using NaOH (0.1 M solution). Then 11 mL of above Au-solution was added into 97 mL of MilliQ water which was maintained at 70 °C in advance. After 10 minutes' stirring, 1.0 g of TiO₂ particles was added and the mixtures were stirred for 1h at 70 °C. After cooling to room temperature, the obtained Au-TiO₂nanoparticles were centrifuged (6000 rpm for 15 min), washed three times with MillQ water and dried at 70 °C overnight. In order to prepare Au-TiO₂ doped with varied Au-content, the concentration of AuCl₃ solution was varied.

Biocatalyst preparation

The unspecific peroxygenase from *Agrocybe aegerita* (rAaeUPO) evolved for functional expression in yeast (Molina-Espeja, P., Garcia-Ruiz, E., Gonzalez-Perez, D., Ullrich, R., Hofrichter, M. and Alcalde, M. (2014). Directed evolution of unspecific peroxygenase from *Agrocybe aegerita*. *Applied & Environmental Microbiology* 80: 3496-3507) was produced and purified as described previously. It was expressed in *Pichia pastoris* as described recently.(3, 4) The culture broth with *P. pastoris* cells containing rAaeUPO was clarified by centrifugation at 8000 rpm for 2 hours at 4 °C. The supernatant was filtered through a 20 µm filter and kept at -80°C. rAaeUPO activity was determined to be 652 ± 5 U mg⁻¹ (pH 5.0 in NaPi buffer). One unit of the enzyme activity was defined as the amount of the enzyme catalysing the oxidation of 1 µmol of ABTS per minute.

Protein purification

The supernatant was concentrated (Amicon 10-kDa-cut-off) and dialyzed against 100 mM sodium phosphate, pH 7. AaeUPO was purified using an NGC Chromatography system (Biorad), in one single step. The separation was performed on a Q Sepharose FF 30-mL cartridge with a flow rate of 5 mL min⁻¹. After 90 mL, the retained protein was eluted with a 0–50% NaCl gradient in 450 mL, followed by 50–100% gradient in 50 mL and 100% NaCl in 75 mL. Peroxidase activity was followed by ABTS oxidation in the presence of H₂O₂, and the appropriate fractions were pooled, concentrated and dialyzed against 100 mM sodium phosphate buffer (pH 7). The purification of the UPO was confirmed by sodium dodecyl sulfate (SDS)–PAGE in 12% gels stained with Coomassie brilliant blue R-250 (Sigma). The UV/Vis spectrum of purified rAaeUPO showed Reinheitszahl (Rz: A420/A280) value of 1.6.

Concentration of rAaeUPO

The concentration of rAaeUPO was determined using the molar extinction coefficient of $115 \text{ mM}^{-1} \text{ cm}^{-1}$ at 420 nm. Absorption spectrum in the UV/Vis range was recorded in a Biomet5 (Thermo) spectrophotometer (2).

Photoenzymatic reactions

Photochemical enzymatic reactions using rAaeUPO were performed at 30 °C in 1.0 mL of sodium phosphate buffer (NaPi, pH 7.0, 60 mM). Unless mentioned otherwise, 5.0 mg of photocatalyst was firstly suspended in 900 uL of NaPi buffer under sonication (5 min in an ultrasonication bath), 350 nM of AaeAPO and 15mM of substrates (final concentration) were then added to the suspension. The volume of the reaction mixture was adjusted to 1.0 mL in a final step. The reaction vial was closed, and exposed to visible light (Philips 7748XHP 205W, white light bulb) under gentle stirring. The homemade experimental setup is shown in Figure S2. The distance between the reaction vial and bulb is 3.6 cm. At intervals, aliquots were withdrawn, extracted with ethyl acetate (containing 5 mM of 1-octanol/dodecane as internal reference) and analyzed by Gas Chromatography (SHIMADZU).

Photocatalytic steady-state hydrogen peroxide generation

Photocatalytic hydrogen peroxide generation reactions using Au-TiO₂ were performed at 30°C in 1.0 mL of sodium phosphate buffer (NaPi, pH 7.0, 60 mM). Unless mentioned otherwise, 5.0 mg of photocatalyst and 250 mM of methanol were used. The reaction vial was closed, and exposed to the light source (Philips 7748XHP 205 W, white light bulb) under gentle stirring. To analyze the concentration of H₂O₂ a fluorometric method reported by Guilbault was adapted.(5) Horse radish peroxidase (HRP) catalyses the dimerisation of p-hydroxyphenylacetic acid (POHPAA) in the presence of H₂O₂ which yields in a detectable fluorescent product. Lyophilized powder of HRP (1 mg, 163 U/mg, Type II, Sigma) was dissolved in TRIS buffer (12.5 ml, pH 8.8, 1 M, Alfa Aesar). POHPAA (4 mg, Alfa Aesar, recrystallized twice from water) was also dissolved in TRIS buffer (12.5 ml). 12.5 µl of each solution was added to 100 µl of a sample containing H₂O₂ and the fluorescence signal ($\lambda_{\text{ex}} = 315 \text{ nm}$, $\lambda_{\text{em}} = 406 \text{ nm}$, 25°C) was determined in a microplate reader (SynergyMx, BioTek). Before analyzing the H₂O₂ concentration, the samples were first filtered through a PVDF syringe filter (0.2µm, Roth) to remove the TiO₂ particles.

The concentration-time profiles of peroxide formation were analyzed using the kinetic model developed by Kormann et al., see eq. 1.(6) Non-linear regression (Levenberg-Marquardt algorithm) of the experimental data to the model yields the kinetic parameters formation rate k_F and degradation rate k_D .

$$c = \frac{k_F}{k_D} + e^{-k_D t} \left(c_0 - \frac{k_F}{k_D} \right) \quad (1)$$

Quantitative OH-Radical detection via coumarin hydroxylation

Coumarin hydroxylation reactions using Au-TiO₂ were performed at 30°C in 1.0 mL of sodium phosphate buffer (NaPi, pH 7.0, 60 mM). 0.1 mM Coumarin (Aldrich), 5.0 mg of

photocatalyst and 250 mM of methanol were used. The reaction vial was closed and irradiated under gentle stirring. To analyze the concentration of umbelliferone samples were taken and TiO₂ was separated via centrifugation. The fluorescence signal ($\lambda_{\text{ex}} = 332 \text{ nm}$, $\lambda_{\text{em}} = 455 \text{ nm}$, 25°C) of 100 μL of the supernatant was measured in a microplate reader. The amount of OH-radicals was calculated assuming 6.1% of coumarin being hydroxylated to umbelliferone.(7)

Actinometry

Chemical actinometry was performed at 30°C in 1.0 mL of 150 mM potassium ferrioxalate solution (freshly prepared from mixing potassium oxalate and iron(III) chloride and recrystallizing from water) in 50 mM sulfuric acid. The reaction vial was closed and irradiated under gentle stirring in a darkened room to avoid interference from other light sources. The amount of formed Fe(II) was determined via the absorbance of the ferrioxalate complex. 25 μL samples were diluted with 20 μL 0.1% aqueous 1,10-phenanthroline solution, 75 μL of 50 mM sulfuric acid, 50 μL 1 M acetate buffer and adjusted to 200 μL with water. The absorbance at 510 nm was measured in a microplate reader.

With the information of the wavelength-dependent quantum yield $\phi(\lambda)$ of the photochemical ferrioxalate-reduction to Fe(II) (obtained via linear interpolation of the values given in Ref (8) and transmission spectrum of the ferrioxalate solution in the reaction vessel $T(\lambda)$ and the photon flux distribution of the lamp $I(\lambda)$, the photon flux density φ was calculated by integrating over the whole wavelength range, eq. 2. The resulting photon flux density is 792 $\mu\text{E L}^{-1} \text{ s}^{-1}$ which amounts to a radiant flux density of 157 W L^{-1} .

$$\varphi = \int \phi(\lambda) \cdot I(\lambda) \cdot (1 - T(\lambda)) d\lambda \quad (2)$$

Characterization of Au-TiO₂

The structures of the synthesized photocatalysts were characterized by a Bruker D8 Advance X-ray diffractometer using Co-K α radiation ($\lambda = 1.789 \text{ \AA}$) at 35 kV and 40 mA. The data were collected from $2\theta = 5.0^\circ$ - 80° with a step size of 0.020° and a counting time of 0.5 s per step. The particle size and morphology were analyzed by using Philips CM30TTEM.

Semi-preparative synthesis

Reaction condition: 100 mL reaction mixture, 10 mg/mL rutile Au-TiO₂, 200 nM of UPO, 250 mM methanol and 20 mM ethyl benzene. All the mixture was placed in a 100 mL glass bottle. The mixture was irradiated for 93 hours under visible light at 30 °C. 12.26 mM of (*R*)-1-phenylethanol and 1.34 mM of acetophenone were obtained after 93 h.

The reaction mixture was then firstly centrifuged to recover the photocatalyst. The supernatant was then extracted with DCM (3 \times), dried over anhydrous MgSO₄ and purified with flash column chromatography. Finally, 0.1074g of product was achieved with 97.2 % ee and 51% isolated yield.

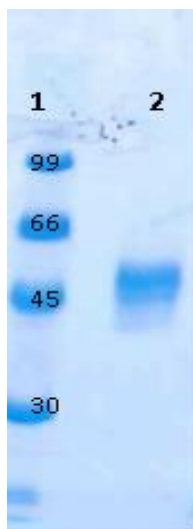


Fig. S3. Purification of UPO. Lane 1 standard (99 kDa, 66 kDa, 45 kDa and 30 kDa) and lane 2 purified enzyme).

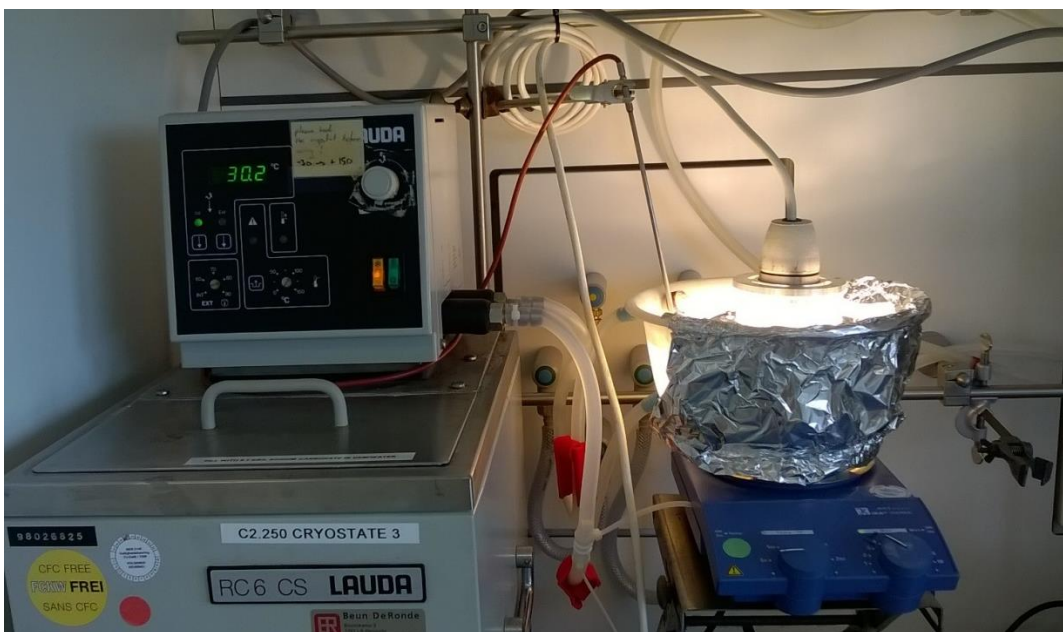


Fig. S2. Image of homemade photocatalytic setup.

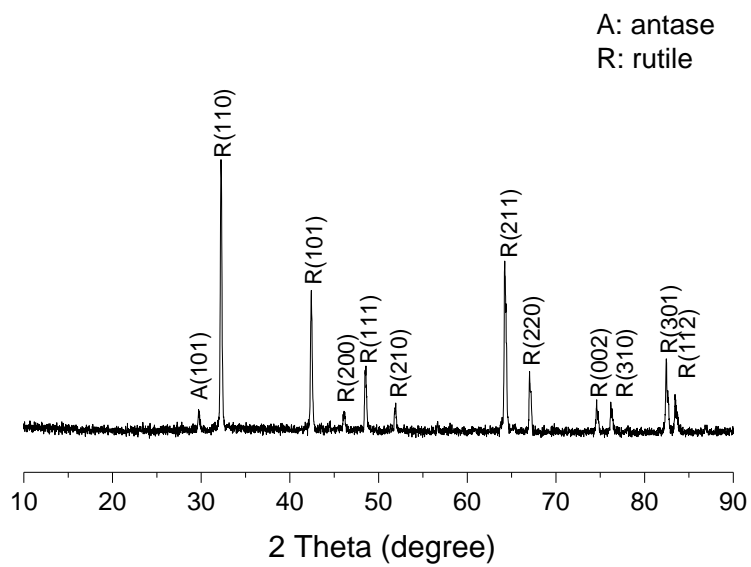


Fig. S3. XRD pattern of rutile Au-TiO₂ photocatalyst.

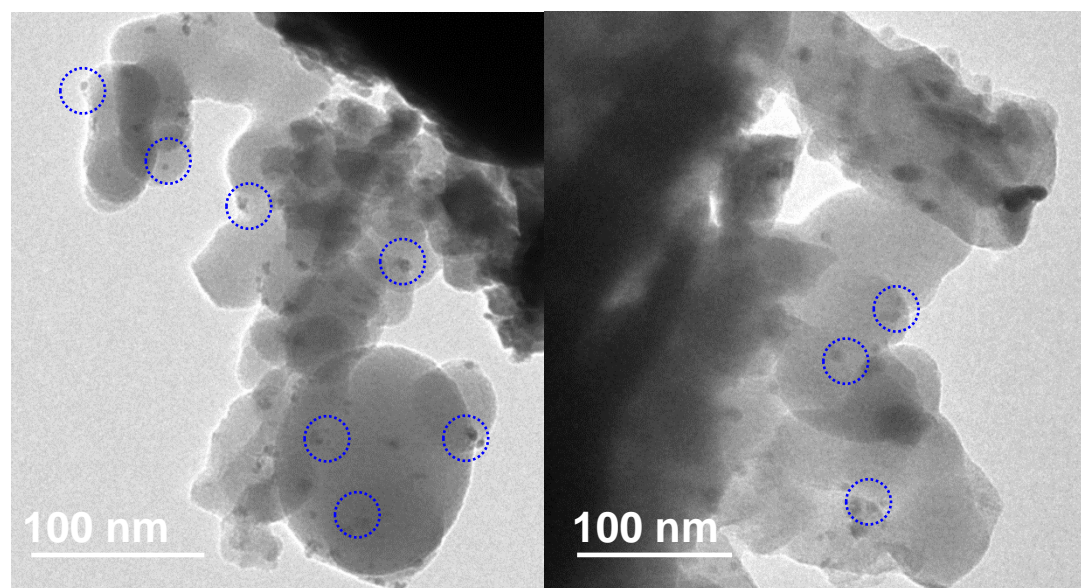


Fig. S4. TEM of rutile Au-TiO₂ photocatalyst.

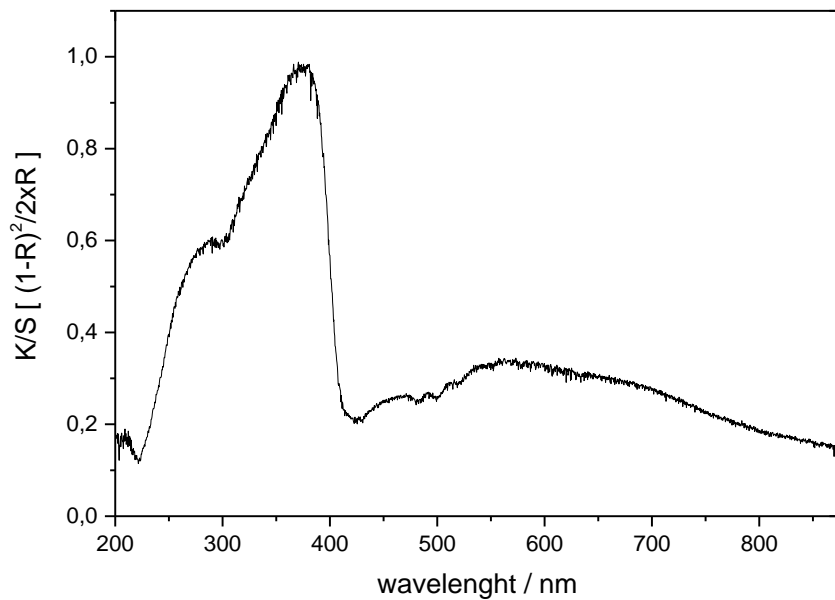


Fig. S5. Apparent absorption spectrum of the Au-TiO₂ catalyst. The absorption was calculated from the diffuse reflectance spectrum (against BaSO₄ as total reflection standard) using the Kubelka-Munk transform.(9)

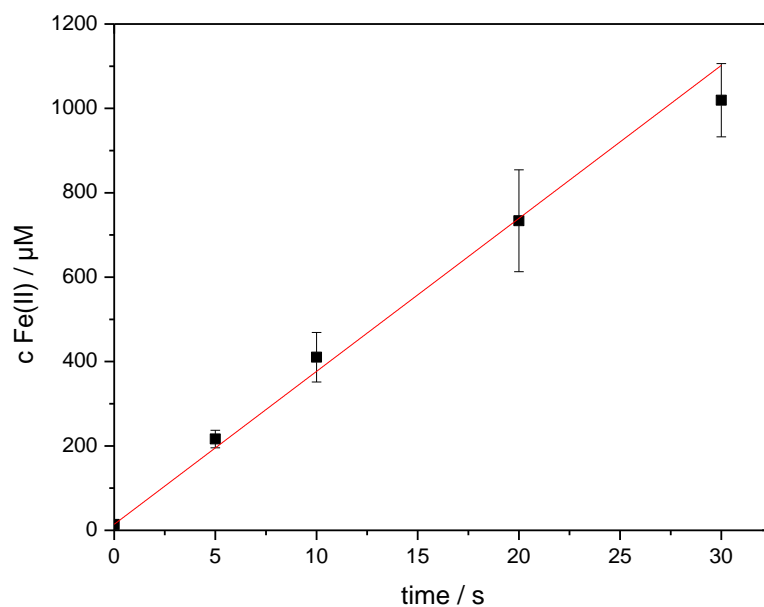


Fig. S6. Average over four different vial positions of time courses of the formation of Fe(II). After illumination of potassium ferrioxalate solution, linear regression yields a slope of $36.3 \mu\text{M s}^{-1}$. Conditions: $[\text{K}_3[\text{Fe}(\text{C}_2\text{O}_4)_3]] = 150 \text{ mM}$ in sulphuric acid (50 mM).

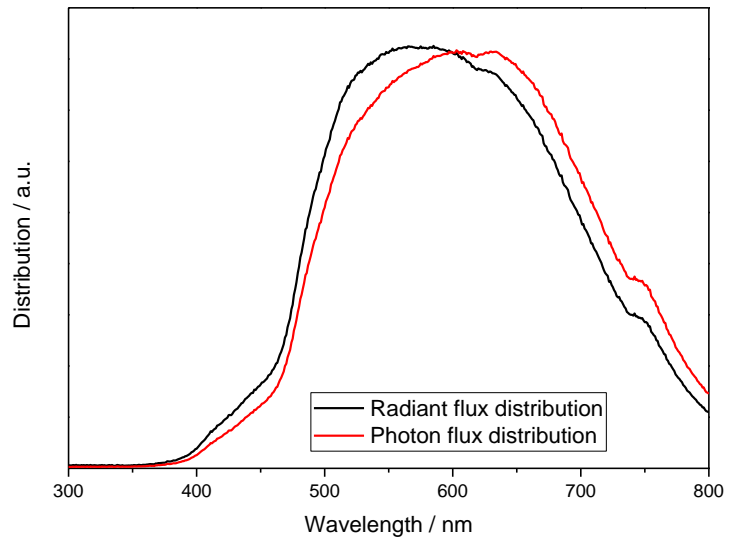


Fig. S7. The radiant flux distribution of the lamp. The measurement used a Ocean Optics FLAME-S-UV-VIS-ES fibre optic spectrophotometer and the calculated photon flux distribution.

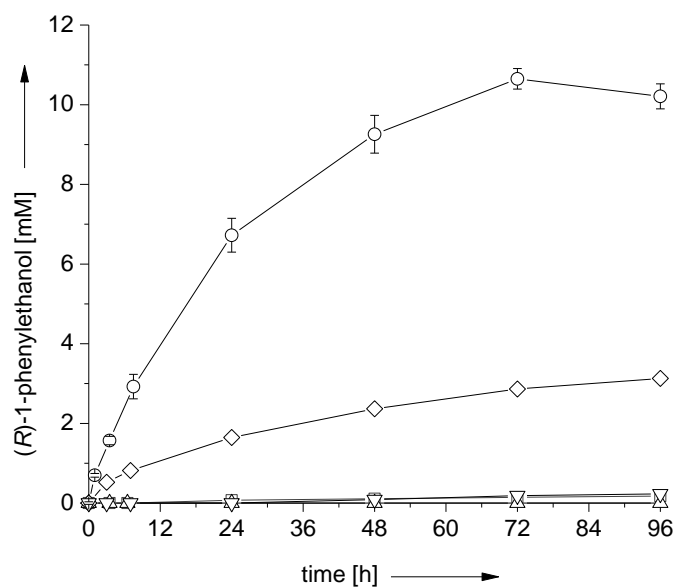


Fig. S8. Product formation of photochemoenzymatic hydroxylation of ethyl benzene to (*R*)-1-phenyl ethanol using rutile Au-TiO₂ as photocatalyst for methanol oxidation (○). Negative controls excluding enzyme (□), light (△), methanol (◇) or rutile Au-TiO₂ (▽). Reaction conditions: [methanol] = 250 mM, [rutile Au-TiO₂] = 5 mg mL⁻¹, [rAaeUPO] = 150 nM and [ethylbenzene] = 15 mM in 60 mM phosphate buffer (pH 7.0) under visible light illumination ($\lambda > 400$ nm). This supporting Figure is corresponding to Figure 1 in the main text.

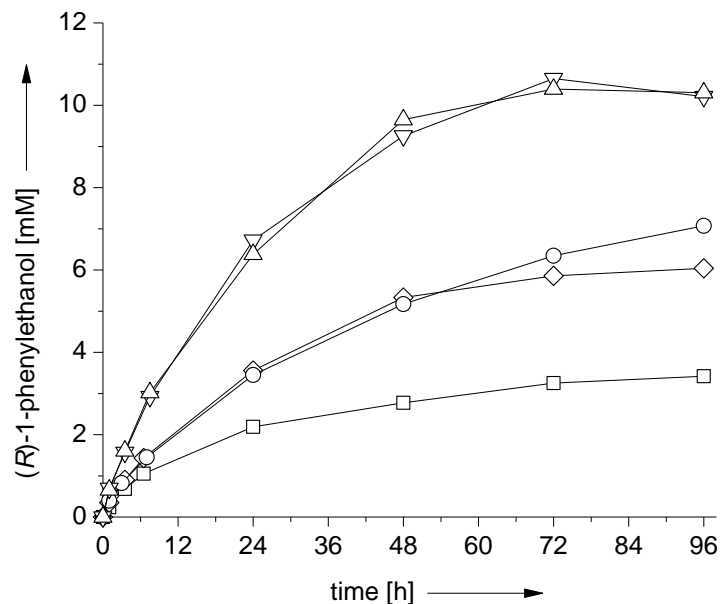


Fig. S9. Product formation of hydroxylation of ethyl benzene using varied methanol concentrations. Conditions: [methanol] = 250 mM (∇, 1% v/v), 100 mM (○, 0.4 % v/v), 50 mM (◇, 0.2 % v/v) and 5 mM (□, 0.02% v/v). [rutile Au-TiO₂] = 5 mg mL⁻¹, [rAaeUPO] = 150 nM, [ethylbenzene] = 15 mM in 60 mM phosphate buffer (pH 7.0) under visible light illumination ($\lambda > 400$ nm).

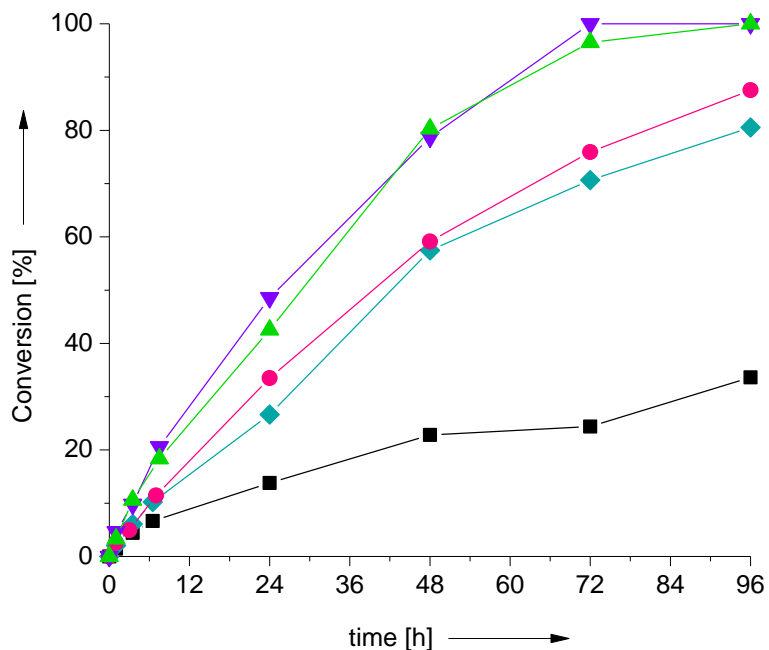


Fig. S10. Conversion of hydroxylation of ethyl benzene using varied methanol concentrations. Conditions: [methanol] = 500 mM (▲, 2% v/v), 250 mM (▼, 1% v/v), 100 mM (●, 0.4 % v/v), 50 mM (◆, 0.2 % v/v) and 5 mM (■, 0.02% v/v). [rutile Au-TiO₂] = 5 mg mL⁻¹, [rAaeUPO] = 150 nM, [ethylbenzene] = 15 mM in 60 mM phosphate buffer (pH 7.0) under visible light illumination ($\lambda > 400$ nm).

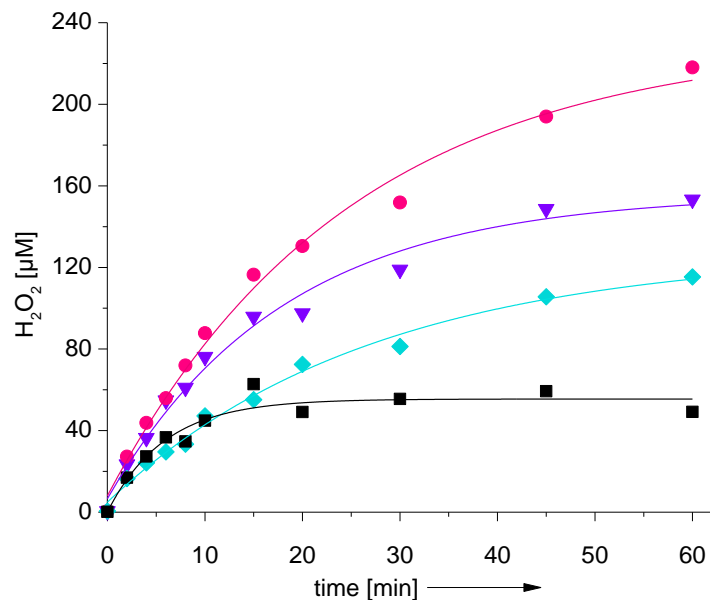


Fig. S11. Steady-state H₂O₂ concentration using varied methanol concentrations. Conditions: [methanol] = 500 mM (▲, 2% v/v), 250 mM (▼, 1% v/v), 100 mM (●, 0.4 % v/v), 50 mM (◆, 0.2 % v/v) and 5 mM (■, 0.02% v/v). [rutile Au-TiO₂] = 5 mg mL⁻¹ in 60 mM phosphate buffer (pH 7.0) under visible light illumination ($\lambda > 400$ nm).

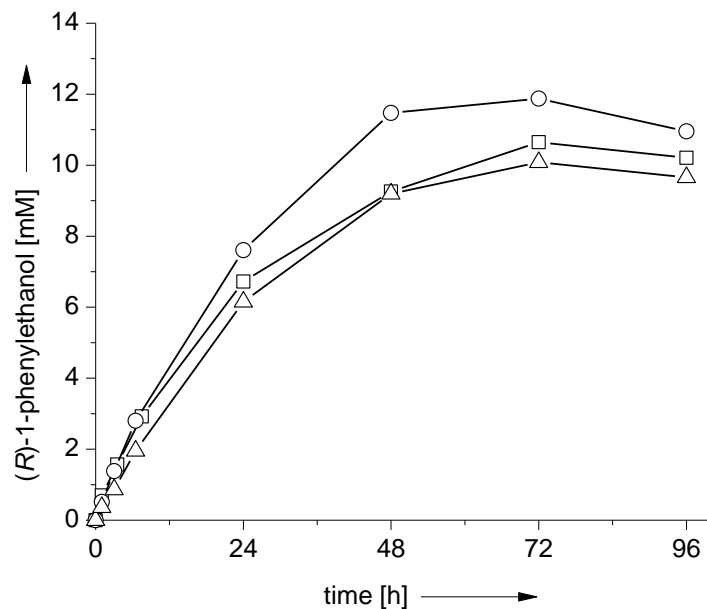


Fig. S12. Product formation of photochemoenzymatic hydroxylation of ethyl benzene using varied rutile Au-TiO₂ concentrations. Conditions: [rAaeUPO] = 150 nM, [methanol] = 250 mM (1% v/v), [rutile Au-TiO₂] = 5 mg mL⁻¹ (□), 10 mg mL⁻¹ (○) and 20 mg mL⁻¹ (△), [ethylbenzene] = 15 mM in phosphate buffer (pH 7.0, 60 mM) under visible light illumination ($\lambda > 400$ nm).

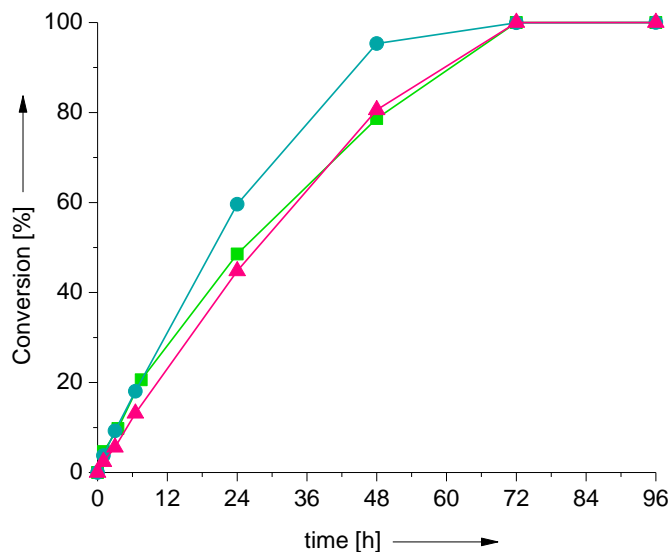


Fig. S13. Conversion of the photochemoenzymatic hydroxylation of ethyl benzene using varied rutile Au-TiO₂ concentrations. Conditions: [rAaeUPO] = 150 nM, [methanol] = 250 mM (1% v/v), [rutile Au-TiO₂] = 5 mg mL⁻¹ (■), 10 mg mL⁻¹ (●) and 20 mg mL⁻¹ (▲), [ethylbenzene] = 15 mM in phosphate buffer (pH 7.0, 60 mM) under visible light illumination ($\lambda > 400$ nm).

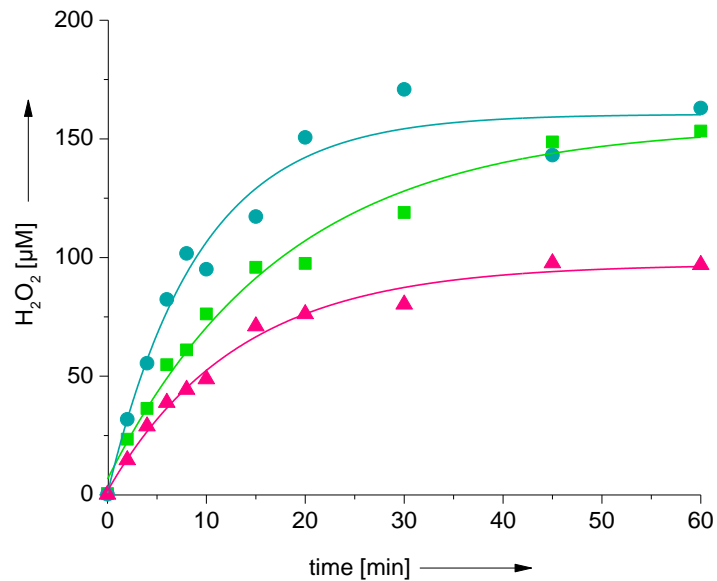


Fig. S14. Steady-state H_2O_2 concentration using varied rutilite Au-TiO_2 concentrations. Conditions: [methanol] = 250 mM (1% v/v), [rutilite Au-TiO_2] = 5 mg mL^{-1} (■), 10 mg mL^{-1} (●) and 20 mg mL^{-1} (▲) in phosphate buffer (pH 7.0, 60 mM) under visible light illumination ($\lambda > 400$ nm).

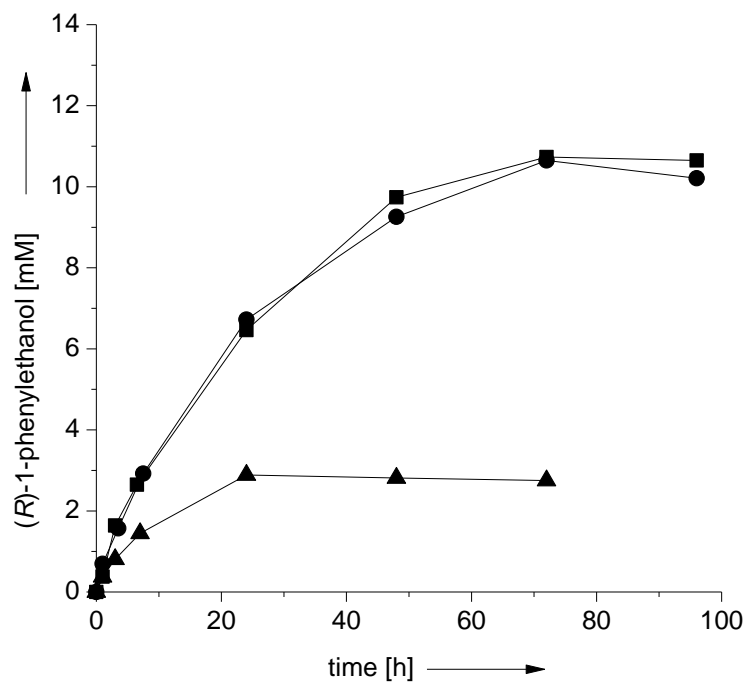


Fig. S15. Product formation of photochemoenzymatic hydroxylation of ethyl benzene using varied *rAaeUPO* concentrations. Conditions: [*rAaeUPO*] = 350 nM(■), 150 nM(●) and 50 nM(▲), [methanol] = 250 mM (1% v/v), rutile Au-TiO₂] = 5 mg mL⁻¹, [ethylbenzene] = 15 mM in 60 mM phosphate buffer (pH 7.0) under visible light illumination ($\lambda > 400$ nm).

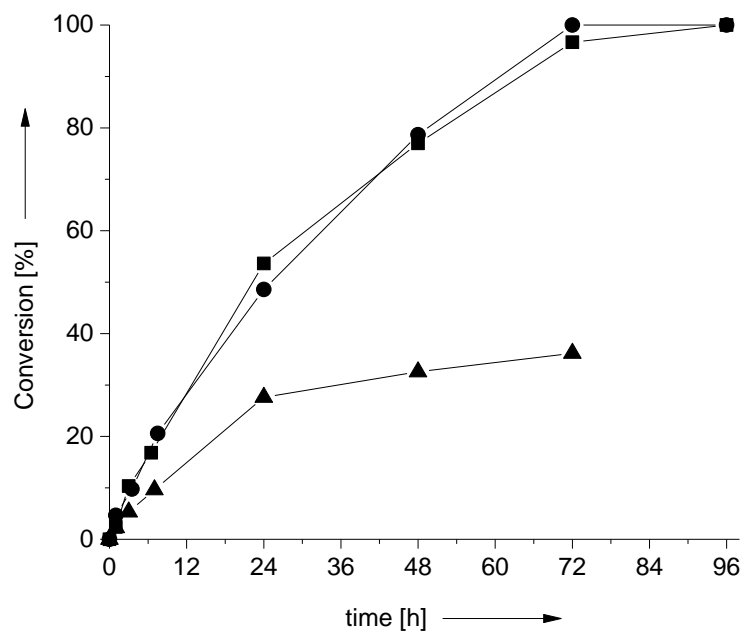


Fig. S16. Conversion of photochemoenzymatic hydroxylation of ethyl benzene using varied *rAaeUPO* concentrations. Conditions: [*rAaeUPO*] = 350 nM(■), 150 nM(●) and 50 nM(▲), [methanol] = 250 mM (1% v/v), rutile Au-TiO₂] = 5 mg mL⁻¹, [ethylbenzene] = 15 mM in 60 mM phosphate buffer (pH 7.0) under visible light illumination ($\lambda > 400$ nm).

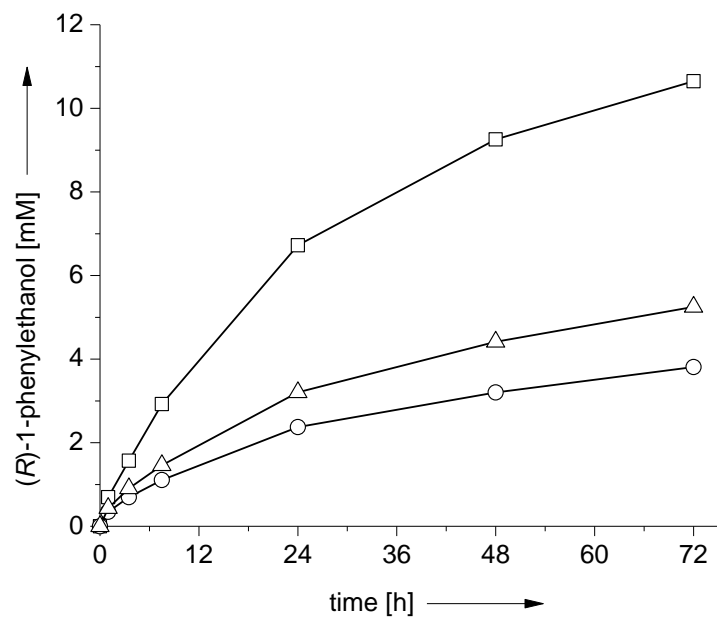


Fig. S17. Product formation of photochemoenzymatic hydroxylation of ethyl benzene using rutile Au-TiO₂ and other alcohols. Using ethanol (○), isopropanol (△) and methanol (□). Conditions: [rAaeUPO] = 150 nM, [rutile Au-TiO₂] = 5 mg mL⁻¹, [ethylbenzene] = 15 mM in phosphate buffer (pH 7.0, 60 mM) under visible light illumination ($\lambda > 400$ nm).

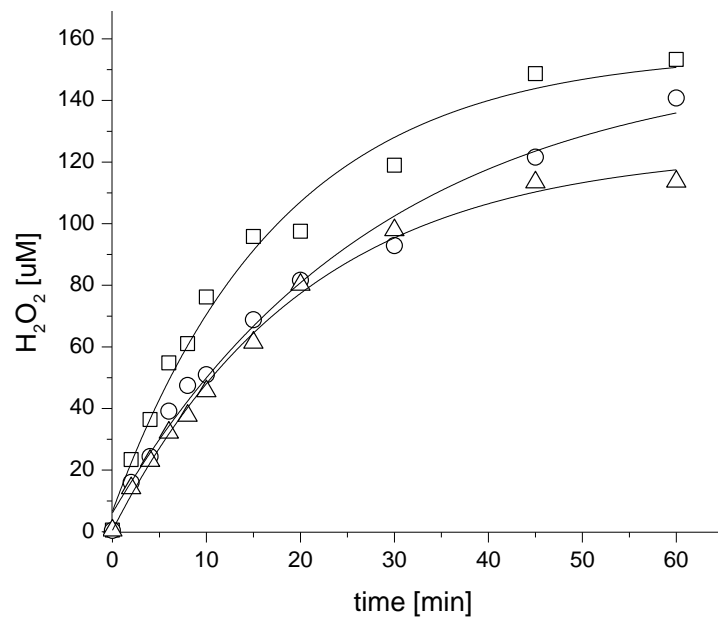


Fig. S18. Steady-state H_2O_2 concentration using various alcohols. Using methanol (\square) ethanol (\circ) isopropanol (\triangle). Conditions: [alcohol] = 250 mM (1% v/v), [rutile Au-TiO₂] = 5 mg mL⁻¹ in phosphate buffer (pH 7.0, 60 mM) under illumination at 30°C.

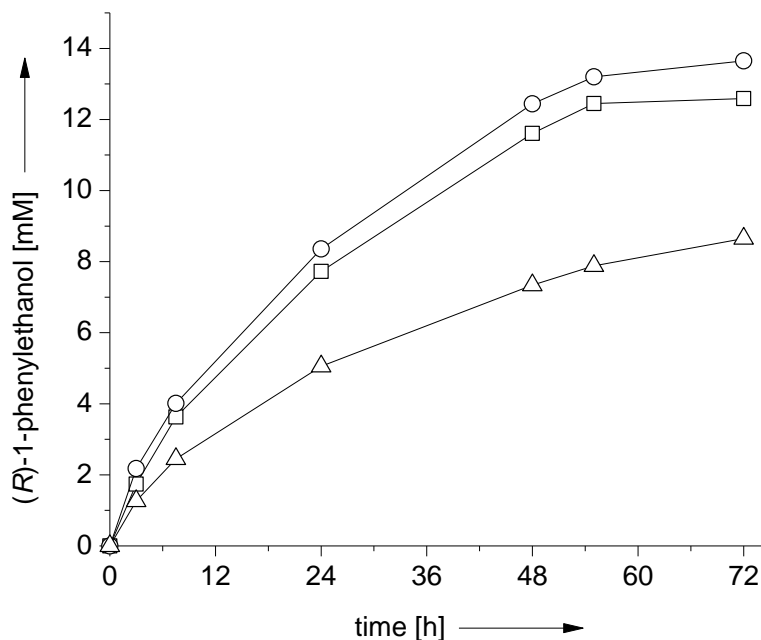


Fig. S19. Product formation of photochemoenzymatic hydroxylation of ethyl benzene using rutile Au-TiO₂ and other hole scavengers: formaldehyde (○), formic acid (△) and sodium formate (□). Conditions: [AaeUPO] = 150 nM, [rutile Au-TiO₂] = 5 mg mL⁻¹, [ethylbenzene] = 15 mM in phosphate buffer (pH 7.0, 60 mM) under visible light illumination ($\lambda > 400$ nm). Reactions using formic acid were performed in phosphate buffer (pH 7.0, 500 mM).

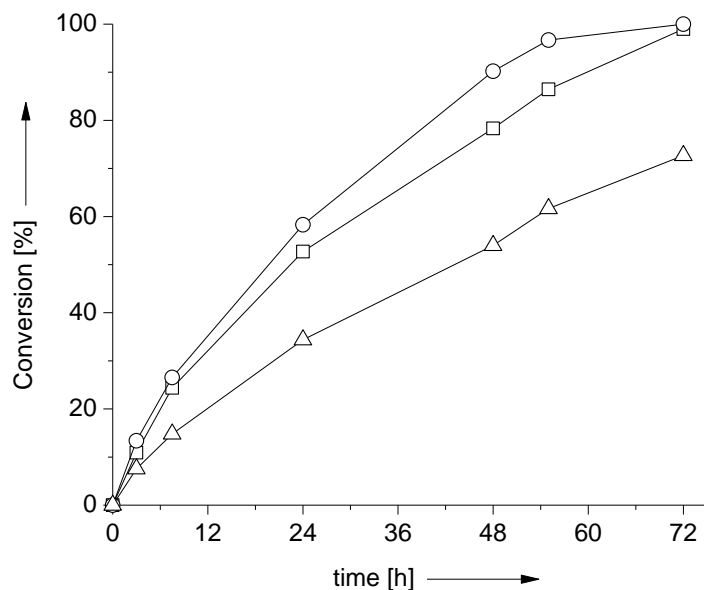


Fig. S20. Conversion of the photochemoenzymatic hydroxylation of ethyl benzene using rutile Au-TiO₂ and other hole scavengers: formaldehyde (○), sodium formate (□) and formic acid(△). Conditions: [rAaeUPO] = 150 nM, [rutile Au-TiO₂] = 5 mg mL⁻¹, [ethylbenzene] = 15 mM in phosphate buffer (pH 7.0, 60 mM) under visible light illumination ($\lambda > 400$ nm). Reactions using formic acid were performed in phosphate buffer (pH 7.0, 500 mM).

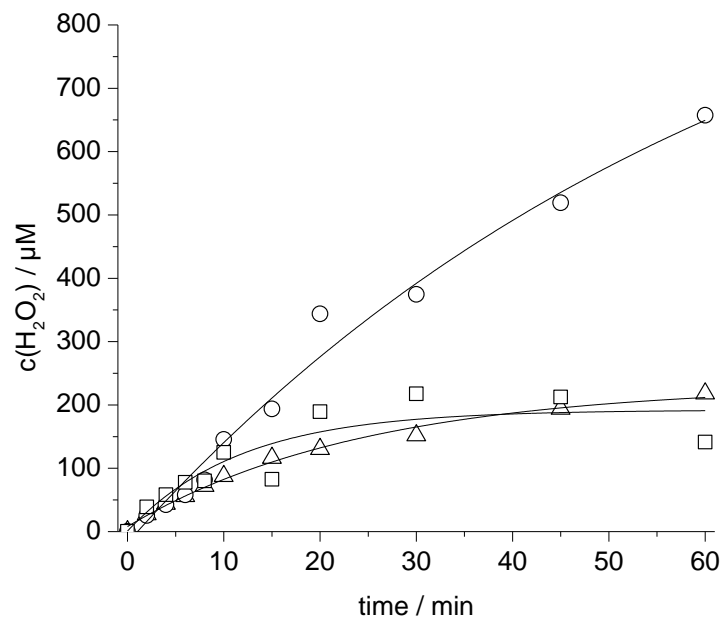


Fig. S21. Steady-state H_2O_2 concentration using rutile Au-TiO_2 and other hole scavengers: formaldehyde (\circ), sodium formate (\square) and formic acid (\triangle). Conditions: $[\text{rutile Au-TiO}_2] = 5 \text{ mg mL}^{-1}$ in phosphate buffer (pH 7.0, 60 mM) under visible light illumination ($\lambda > 400 \text{ nm}$). Reactions using formic acid were performed in phosphate buffer (pH 7.0, 500 mM).

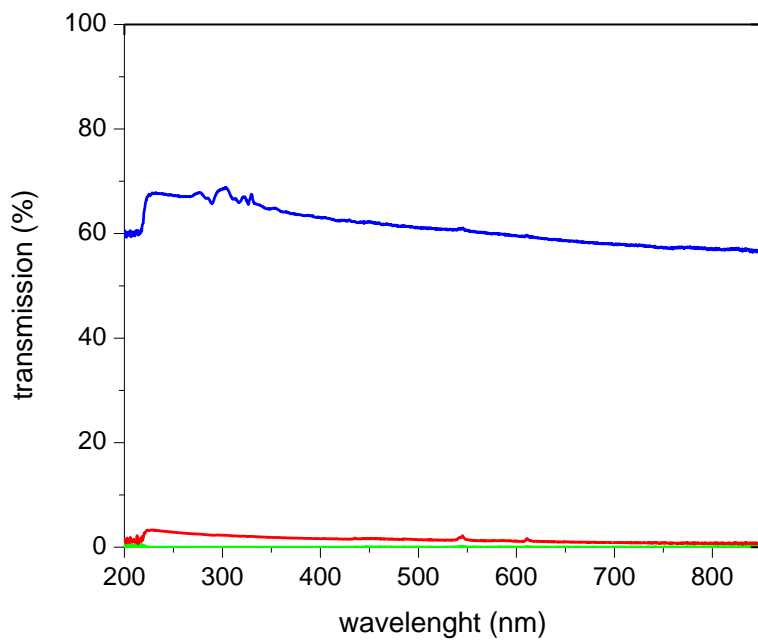


Fig. S22. The transmission spectra (light penetration depth) of the suspensions with 0.005 (blue), 0.5 (red) and 5 g L⁻¹ (green) Au-TiO₂ concentration.

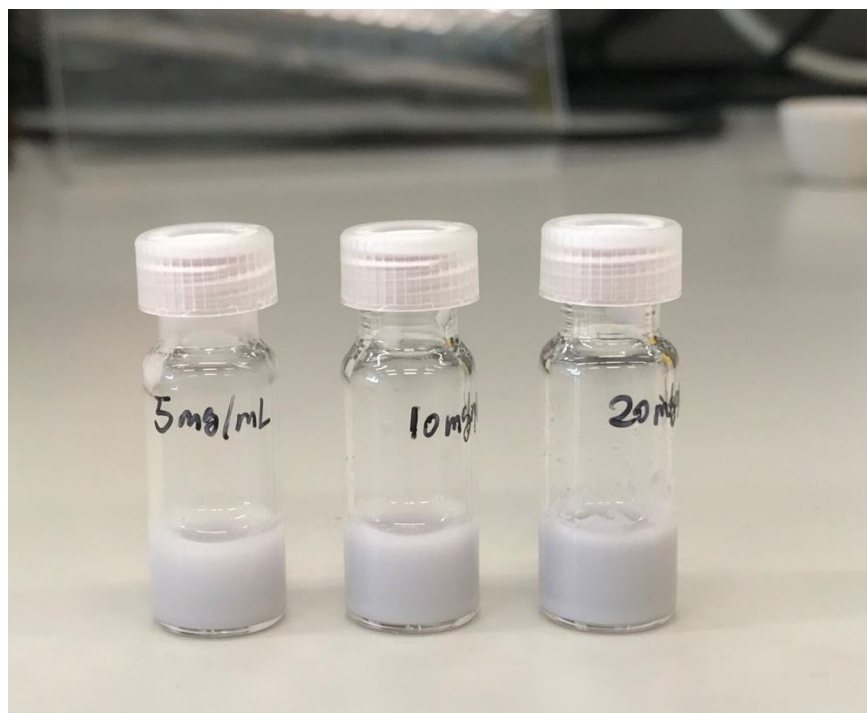


Fig. S23. Transparency of the suspensions with 5, 10 and 20 mg mL⁻¹ from left to right. The picture is guides to the eye.

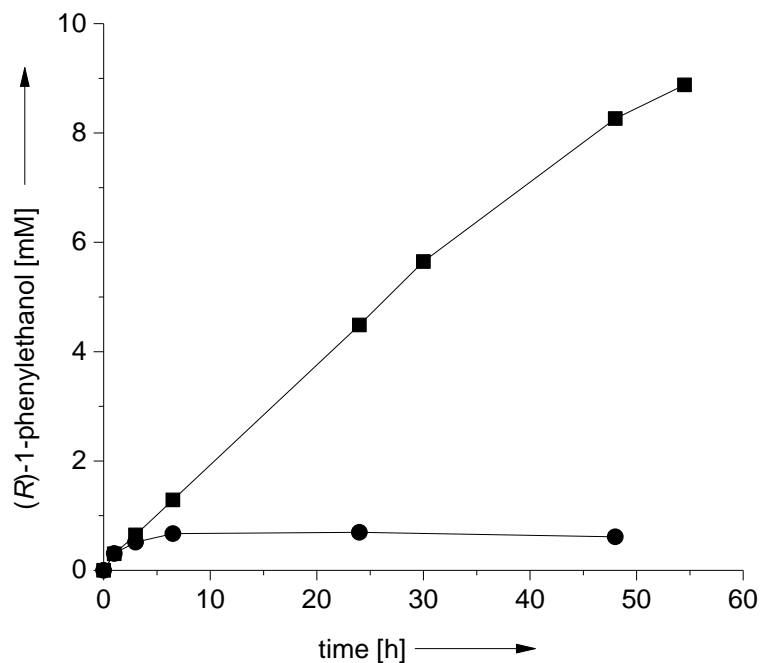


Fig. S24. Product formation of hydroxylation of ethyl benzene using anatase Au-TiO₂ with (■) and without methanol (●). Conditions: [methanol] = 250 mM (1% v/v), [anatase Au-TiO₂] = 5 mg mL⁻¹, [rAaeUPO] = 350 nM, [ethylbenzene] = 15 mM in 60 mM phosphate buffer (pH 7.0) under visible light illumination ($\lambda > 400$ nm).

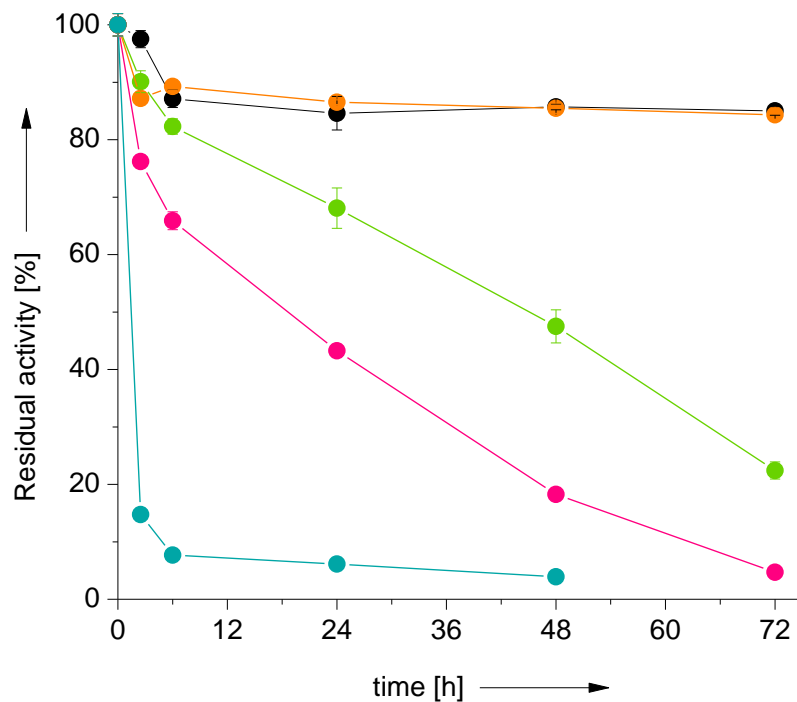


Fig. S25. Residual rAaeUPO activity after incubation in the presence of the photocatalyst and methanol. MeOH+rAaeUPO in dark (●); MeOH+rAaeUPO under light (●); MeOH+rAaeUPO + rutile Au-TiO₂ in dark (●), rAaeUPO + rutile Au-TiO₂ under light (●) and MeOH+rAaeUPO + rutile Au-TiO₂ under light (●). General conditions: phosphate buffer (60 mM, pH 7.0), T= 30 °C, c(rutile Au-TiO₂) = 5 gL⁻¹, c(rAaeUPO) = 150 nM and c(Methanol) = 250 mM.

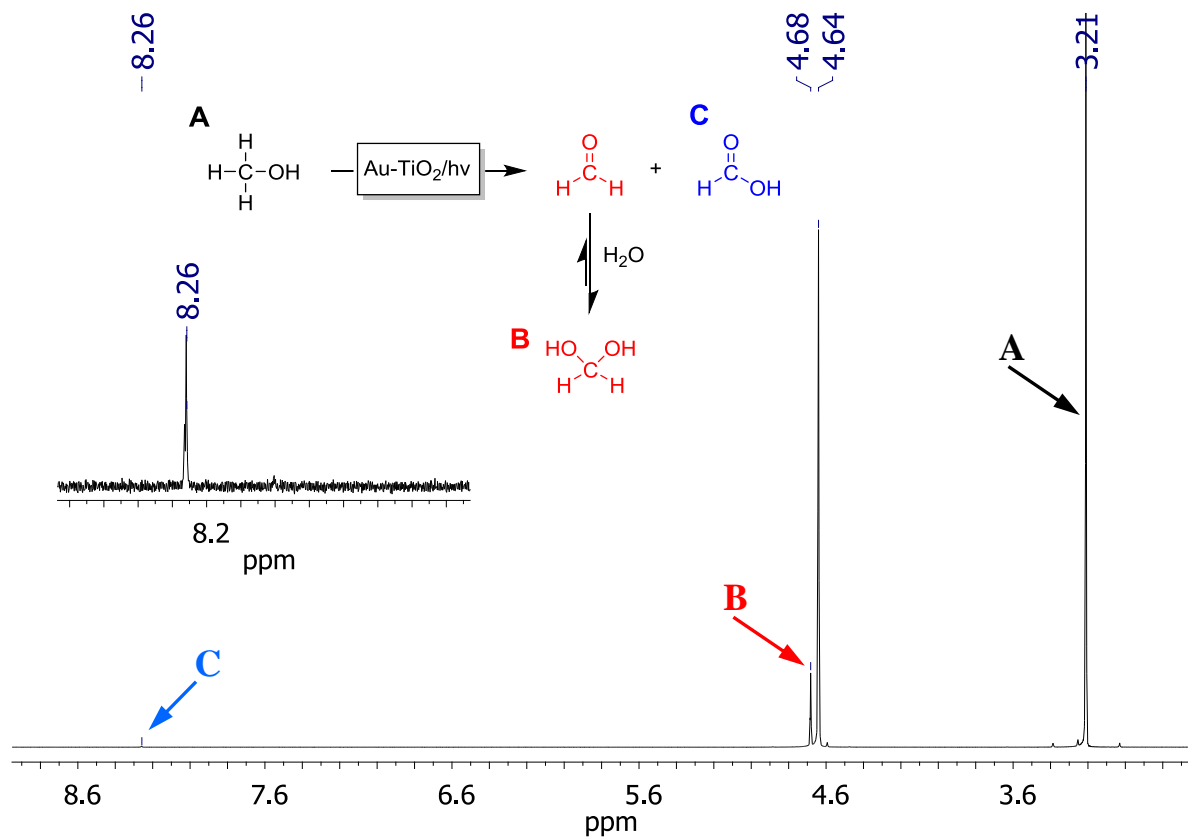


Fig. S26. ^1H NMR of reaction mixture of methanol oxidation in D_2O for 40h (rutile Au-TiO_2 was used). The Agilent 400 MHz NMR was used.

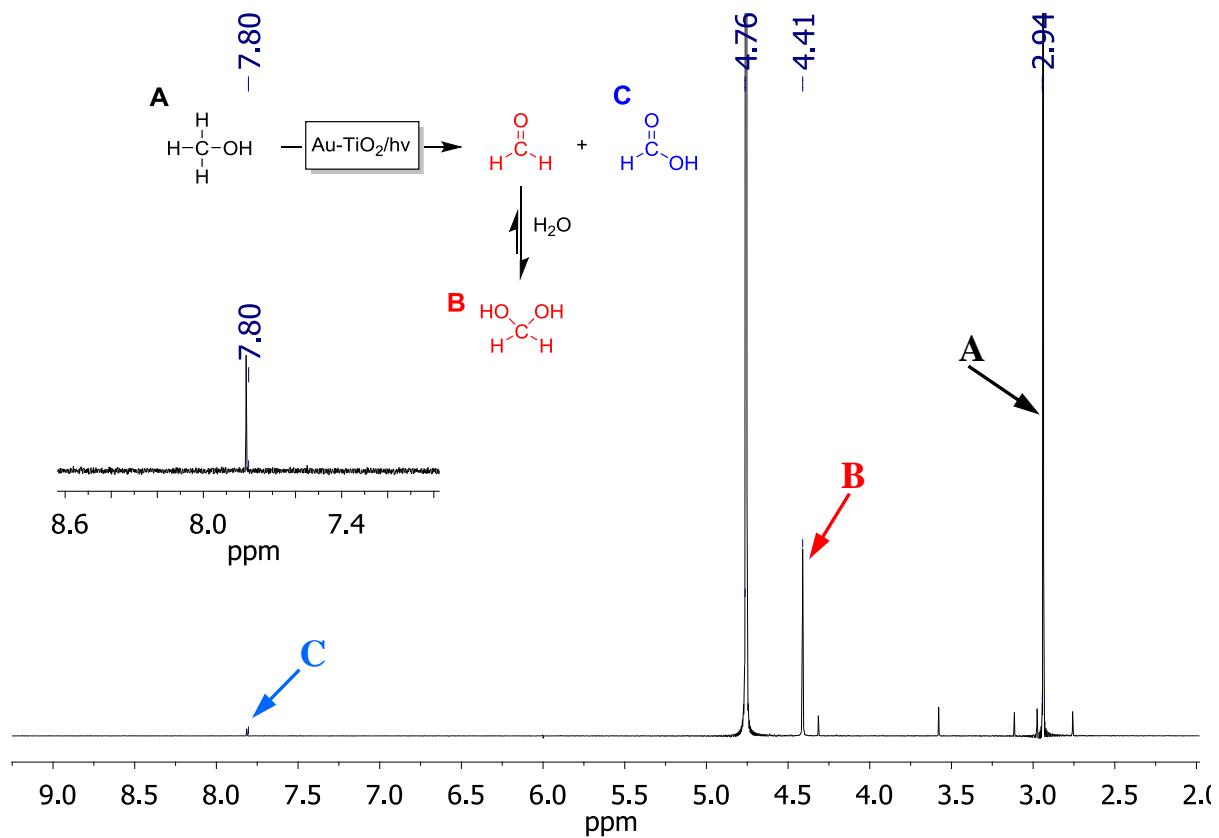


Fig. S27. ^1H NMR of reaction mixture of methanol oxidation in D_2O for 40h (rutile Au-TiO_2 was used). Trifluoroacetic acid was added to shift the hydrogen bonding between D_2O and hydrated formaldehyde. The Agilent 400 MHz NMR was used.

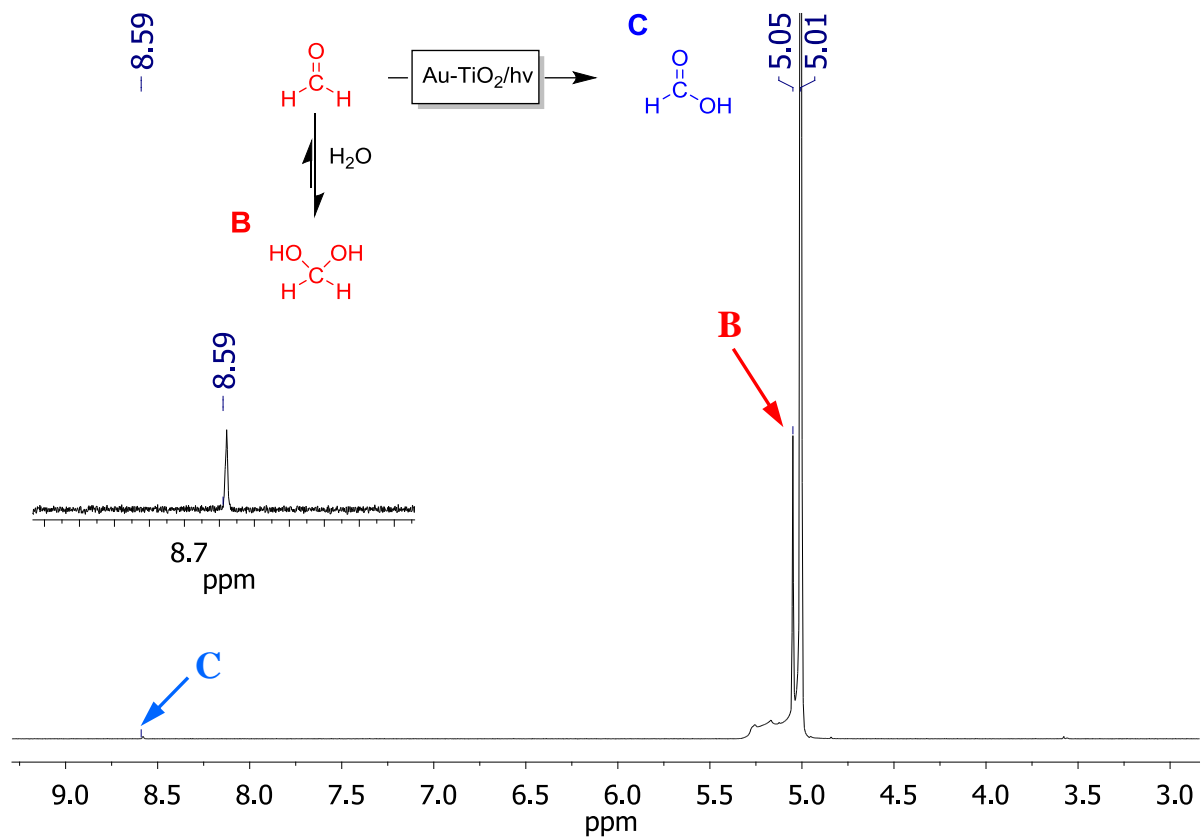


Fig. S28. ^1H NMR of reaction mixture of formaldehyde oxidation in D_2O for 40h (rutile Au-TiO_2 was used). The Agilent 400 MHz NMR was used.

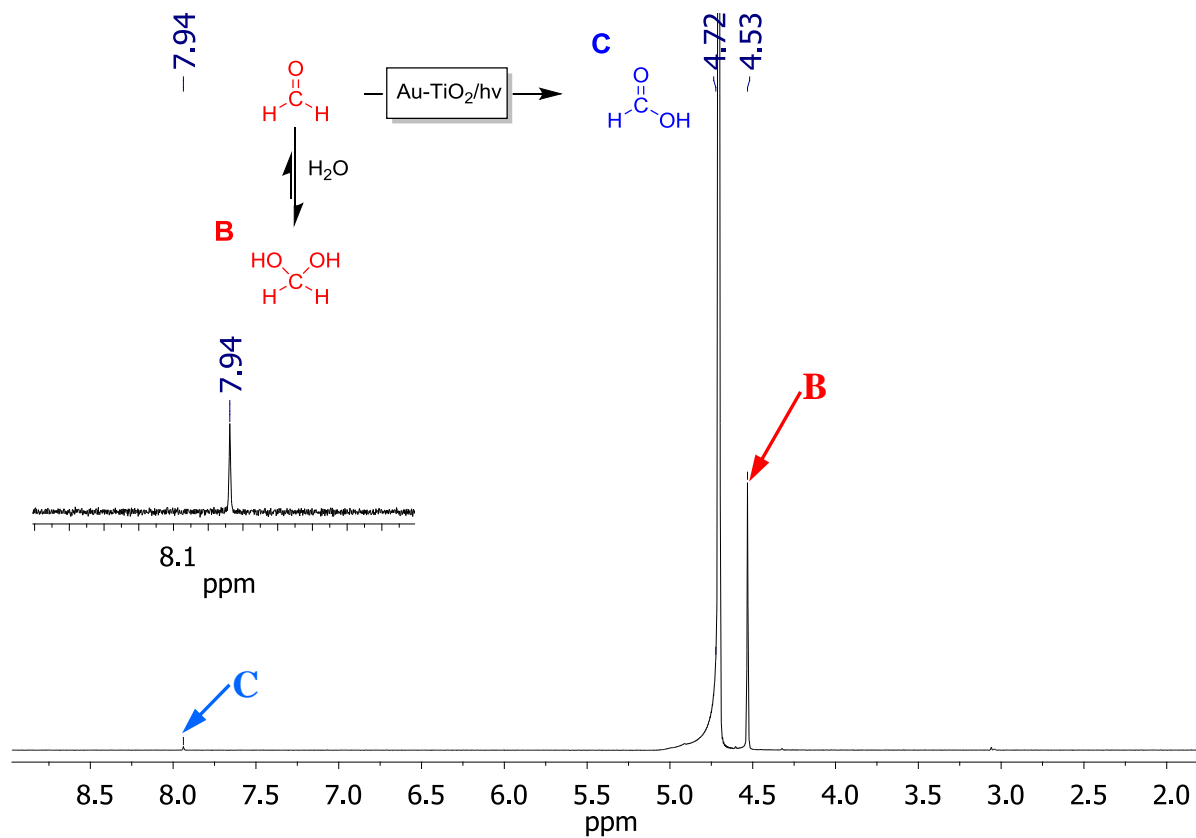


Fig. S29. ^1H NMR of reaction mixture of formaldehyde oxidation in D_2O for 40h (rutile Au-TiO_2 was used). Trifluoroacetic acid was added to shift the hydrogen bonding between D_2O and hydrated formaldehyde. The Agilent 400 MHz NMR was used.

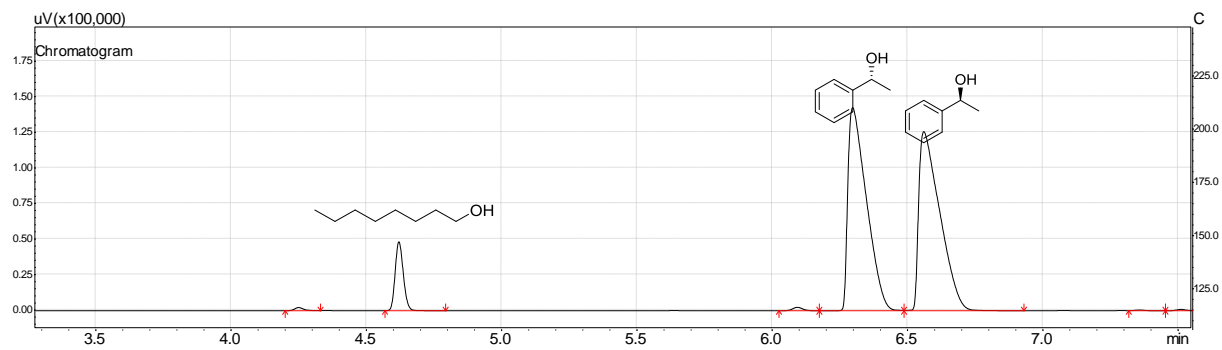


Fig. S30. Representative GC chromatogram of the racemic 1-phenyl ethanol.

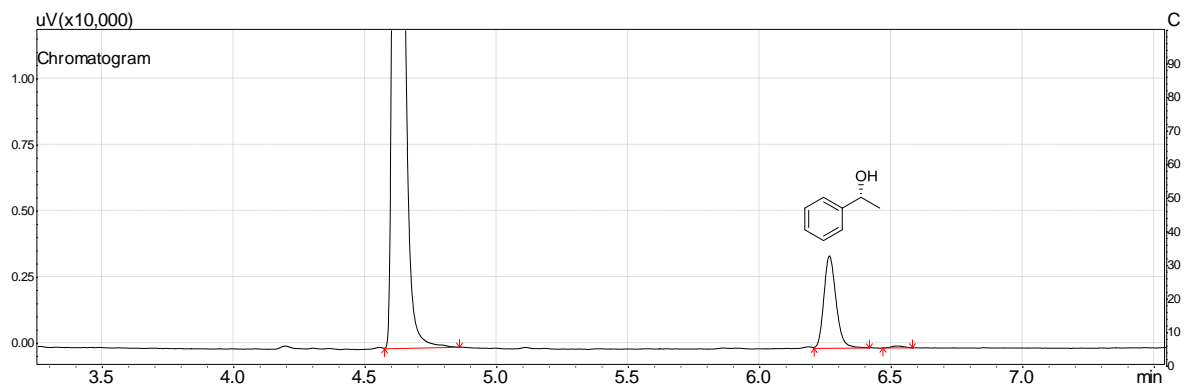


Fig. S31. Representative GC chromatogram of the *Aae*UPO-catalysed oxyfunctionalization of ethyl benzene to (*R*)-1-phenyl ethanol driven by rutile Au-TiO₂ catalyzed water oxidation.

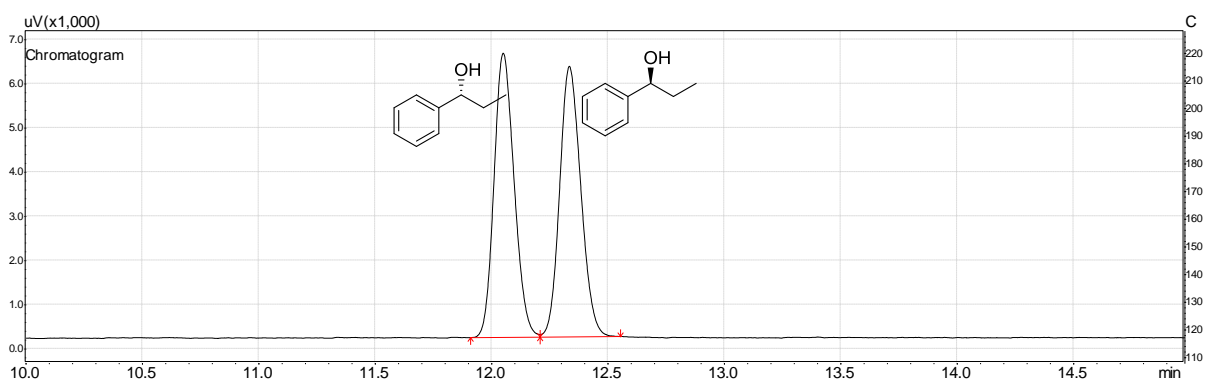


Fig. S32. Representative GC chromatogram of the racemic 1-phenyl-1-propanol.

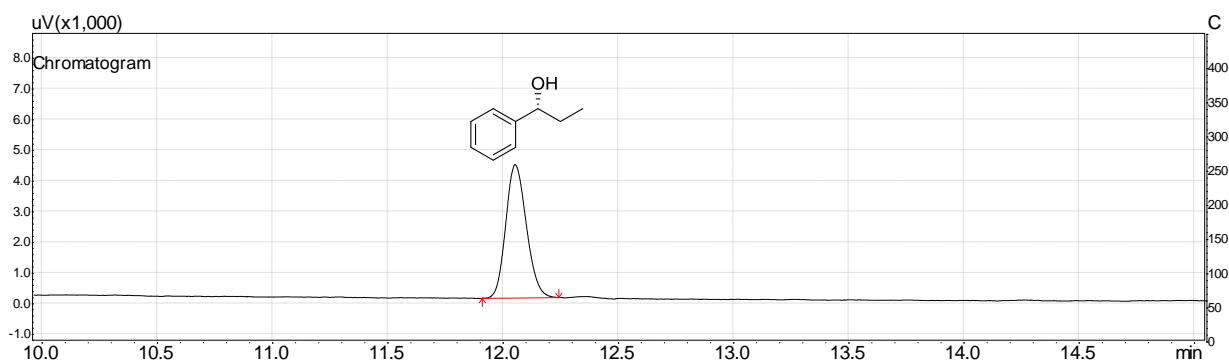


Fig. S33. Representative GC chromatogram of the *Aae*UPO-catalysed oxyfunctionalization of propylbenzene to (*R*)- 1-phenyl-1-propanol driven by rutile Au-TiO₂catalyzed water oxidation.

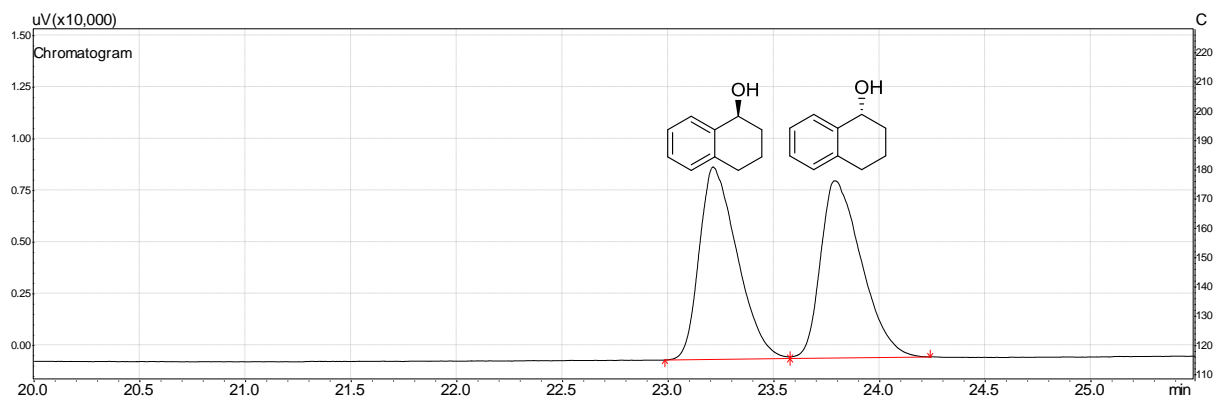


Fig. S34. Representative GC chromatogram of the racemic 1,2,3,4-tetrahydro-1-naphthol.

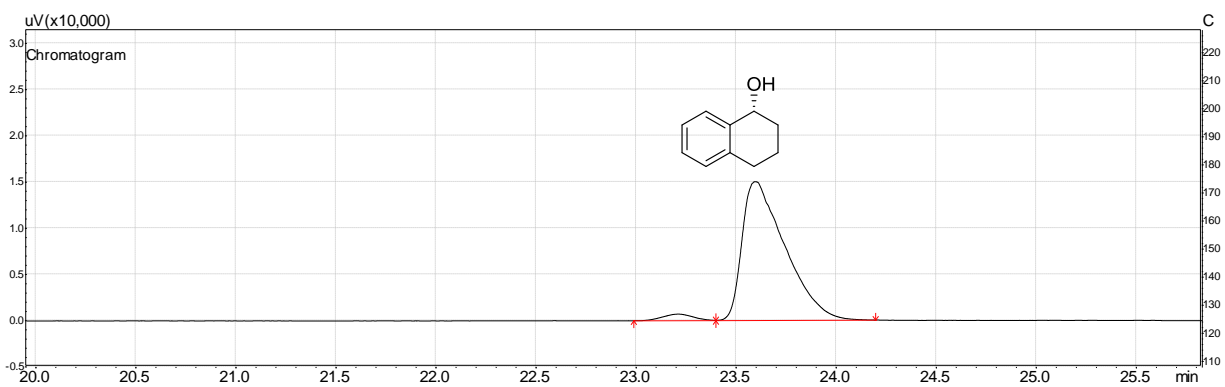


Fig. S35. Representative GC chromatogram of the *Aae*UPO-catalysed oxyfunctionalization of 1,2,3,4-tetrahydronaphthalene driven by rutile Au-TiO₂catalyzed water oxidation.

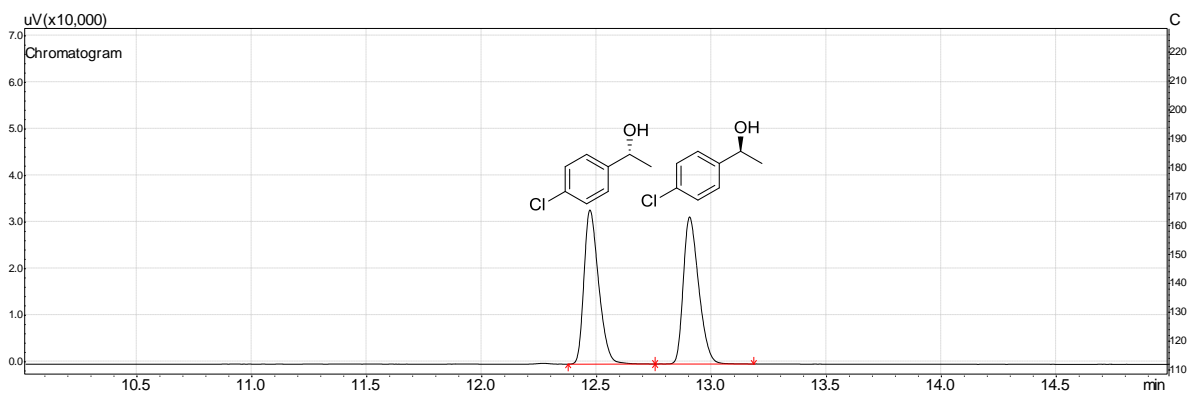


Fig. S36. Representative GC chromatogram of the racemic 4-chloro-1-phenylethanol.

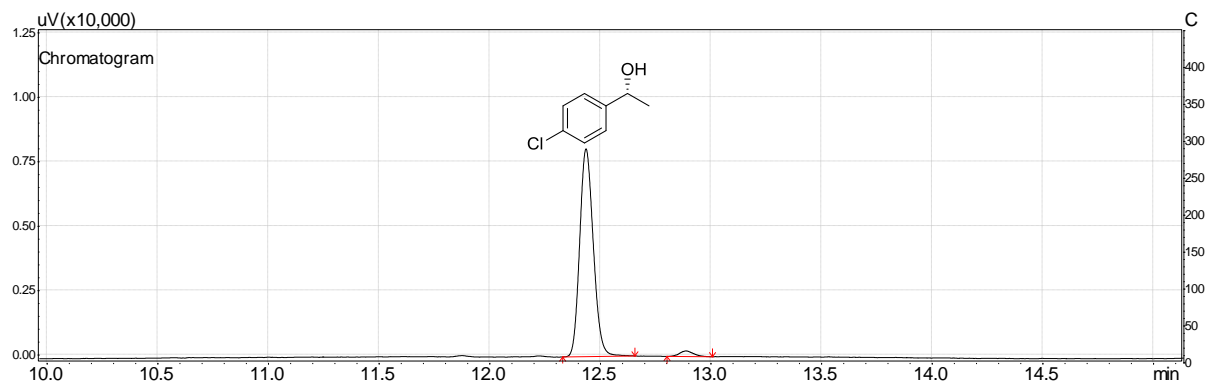
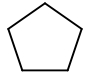
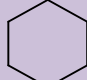
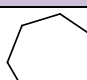
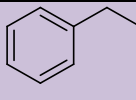
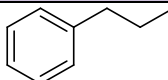
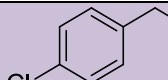
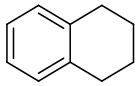
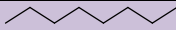


Fig. S37. Representative GC chromatogram of the *Aae*UPO-catalysed oxyfunctionalization of 4-chloro- ethyl benzene driven by rutile Au-TiO₂catalyzed water oxidation.

Table S1.
Details of GC analysis.

Substrate	Analysis, column ^[a]	T_R [min] ^[b]	Temperature profile
 cyclopentane	Column A	cyclopentanol 7.83 cyclopentanone 6.33 IS 11.68	90 °C hold 3 min, 10 °C /min to 180 °C hold 1 min, 30 °C /min to 230 °C hold 1 min.
 cyclohexane	Column A	cyclohexanol 9.57 cyclohexanone 8.24 IS 11.68	90 °C hold 3 min, 10 °C /min to 180 °C hold 1 min, 30 °C /min to 230 °C hold 1 min.
 cycloheptane	Column A	cycloheptanol 12.08 cycloheptanone 10.47 IS 11.68	90 °C hold 3 min, 10 °C /min to 180 °C hold 1 min, 30 °C /min to 230 °C hold 1 min.
 Ethyl benzene	Quantification: Column A Enantiomeric excess: Column B	Quantification: ethylbenzene 2.95 1-phenylethanol 9.06 acetophenone 7.55 Enantiomeric excess: (<i>R</i>)-1-phenylethanol 14.96 (<i>S</i>)-1-phenylethanol 15.95	Quantification: 130 °C hold 3 min, 30 °C /min to 200 °C hold 4.5 min, 30 °C /min to 250 °C hold 1.5 min. Enantiomeric excess: 100 °C hold 4 min, 10 °C /min to 120 °C hold 10 min, 25 °C /min to 215 °C hold 1.3 min. Split ratio 50.
 propylbenzene	Quantification: Column A Enantiomeric excess: Column B	Quantification: propylbenzene 3.97 1-Phenyl-1-propanol 12.26 1-phenylpropanone 10.21 IS 7.07 Enantiomeric excess: (<i>R</i>)-1-Phenyl-1-propanol 12.05 (<i>S</i>)-1-Phenyl-1-propanol 12.33	Quantification: 120 °C hold 2 min, 15 °C /min to 180 °C hold 3 min, 30 °C /min to 200 °C hold 3 min, 30 °C /min to 245 °C hold 1 min. Enantiomeric excess: 120 °C hold 3 min, 5 °C /min to 135 °C hold 8 min, 25 °C /min to 210 °C hold 1 min. Split ratio 40.
 4-chloro-ethylbenzene	Quantification: Column A Enantiomeric excess: Column B	Quantification: 4-chloro-ethylbenzene 4.08 4-chloro-1-phenylethanol 10.17 4-Cl-actonphenone 13.81 IS 4.81 Enantiomeric excess: (<i>R</i>)-4-chloro-1-phenylethanol	Quantification: 150 °C hold 1.5 min, 30 °C /min to 180 °C hold 4 min, 30 °C /min to 210 °C hold 3 min, 30 °C /min to 225 °C hold 3.5 min, 30 °C /min to 245 °C hold 1.5 min. Enantiomeric excess: 120 °C hold 3 min, 10 °C /min to

		12.47 (<i>S</i>)-4-chloro-1-phenylethanol 12.91	150 °C hold 4 min, 10 °C /min to 165 °C hold 3.5 min, 25 °C /min to 210 °C hold 2 min. Split ratio 40.
 (1,2,3,4- tetranaphthalene)	Quantification: Column A Enantiomeric excess: Column B	Quantification: 1,2,3,4-tetranaphthalene 7.14 α -Tetralol 16.15 α -Tetralone 14.65 IS 6.70 Enantiomeric excess: (<i>R</i>)- α -Tetralol 23.95 (<i>S</i>)- α -Tetralol 23.38	Quantification: 130 °C hold 3 min, 15 °C /min to 180 °C hold 1.3 min, 15 °C /min to 225 °C hold 6 min, 30 °C /min to 245°C hold 1 min. Enantiomeric excess: 120 °C hold 3 min, 5 °C /min to 140 °C hold 19 min, 25 °C /min to 210 °C hold 2.5 min. Split ratio 40.
 octane	Quantification: Column A Enantiomeric excess: [d] Column B	Quantification: 2-octanol 4.96 1-octanol 6.65 IS 3.13 ^[c] Enantiomeric excess: ^[d] (<i>R</i>)-2-octanol 8.87 (<i>S</i>)-2-octanol 7.97	Quantification: 130 °C hold 3 min, 30 °C /min to 170 °C hold 2.7 min, 30 °C /min to 240 °C hold 1.2 min. Enantiomeric excess: 100 °C hold 4 min, 10 °C /min to 120 °C hold 3.2 min, 25 °C /min to 215 °C hold 2 min. Split ratio 50.

^[a] Column A: CP Wax 52CB column (25 m \times 0.25 mm \times 1.2 μ m), FID, N₂ is the carrier gas; Column B: ChiralsilDex CB column (25 m \times 0.32 mm \times 0.25 μ m), FID, He is the carrier gas. Column C: Cpsil 5 CB: (50 m \times 0.53mm \times 1.0 μ m), FID, N₂ is the carrier gas. ^[b]1-Octanol (5mM in ethyl acetate) is used as internal standard (IS) except otherwise note. ^[c]dodecane (5mM in ethyl acetate) is used as IS. ^[d] In order to measure the ee, 3 mg of *N,N*-Dimethylpyridin-4-amine (DMAP) and 10 μ L of acetic anhydride were added to the ethyl acetate containing the 2-octanol (after the exaction of the samples). The mixture was kept at 30 °C for 45 minutes, then 100 μ L of MilliQ water was added to stop the acetylation. The organic phase was dried over MgSO₂ and measured.

Table S2. Kinetic data of OH radical formation using rutile Au-TiO₂ in the absence and presence of MeOH as a scavenger.

	$k_F(\text{OH}^\bullet) / \text{nM min}^{-1}$
no MeOH	409.8
1% MeOH	2.3

References

1. M. Mifsud, S. Gargiulo, S. Iborra, I. W. C. E. Arends, F. Hollmann, A. Corma, Photobiocatalytic chemistry of oxidoreductases using water as the electron donor. *Nat Commun* **5**, (2014). (DOI: 10.1038/ncomms4145).
2. J. B. Priebe, J. Radnik, A. J. J. Lennox, M.-M. Pohl, M. Karnahl, D. Hollmann, K. Grabow, U. Bentrup, H. Junge, M. Beller, A. Brückner, Solar Hydrogen Production by Plasmonic Au–TiO₂ Catalysts: Impact of Synthesis Protocol and TiO₂ Phase on Charge Transfer Efficiency and H₂ Evolution Rates. *ACS Catal.* **5**, 2137-2148 (2015). (DOI: 10.1021/cs5018375).
3. P. Molina-Espeja, S. Ma, D. M. Mate, R. Ludwig, M. Alcalde, Tandem-yeast expression system for engineering and producing unspecific peroxygenase. *Enzyme Microb. Technol.* **73–74**, 29-33 (2015). (DOI: <http://dx.doi.org/10.1016/j.enzmictec.2015.03.004>).
4. Y. Ni, E. Fernández-Fueyo, A. G. Baraibar, R. Ullrich, M. Hofrichter, H. Yanase, M. Alcalde, W. J. H. van Berkel, F. Hollmann, Peroxygenase-Catalyzed Oxyfunctionalization Reactions Promoted by the Complete Oxidation of Methanol. *Angew. Chem. Int. Ed.* **4 55**, 798-801 (2016). (DOI: 0.1002/anie.201507881).
5. W. Hemrika, R. Renirie, S. Macedo-Ribeiro, A. Messerschmidt, R. Wever, Heterologous Expression of the Vanadium-containing Chloroperoxidase from *Curvularia inaequalis* in *Saccharomyces cerevisiae* and Site-directed Mutagenesis of the Active Site Residues His496, Lys353, Arg360, and Arg490. *J. Biol. Chem.* **274**, 23820-23827 (1999). (DOI: 10.1074/jbc.274.34.23820).
6. C. Kormann, D. W. Bahnemann, M. R. Hoffmann, Photocatalytic production of hydrogen peroxides and organic peroxides in aqueous suspensions of titanium dioxide, zinc oxide, and desert sand. *Environ. Sci. Technol.* **22**, 798-806 (1988). (DOI: 10.1021/es00172a009).
7. J. Zhang, Y. Nosaka, Quantitative Detection of OH Radicals for Investigating the Reaction Mechanism of Various Visible-Light TiO₂ Photocatalysts in Aqueous Suspension. *J. Phys. Chem. C* **117**, 1383-1391 (2013). (DOI: 10.1021/jp3105166).
8. C. G. Hatchard, C. A. C. A. Parker, A new sensitive chemical actinometer - II. Potassium ferrioxalate as a standard chemical actinometer. *Proc. R. Soc. A Math. Phys. Eng. Sci.* **235**, 518-536 (1956). (DOI: 10.1098/rspa.1956.0102).
9. P. Kubelka, F. Munk, Ein beitrag zur optik der farbanstriche. *Zeitschrift für Tech. Phys.* **12**, 593-601 (1931).